Geotextiles and Geomembranes 43 (2015) 56–81

Contents lists available at ScienceDirect

Geotextiles and Geomembranes

journal homepage: www.elsevier.com/locate/geotexmem

Validation of analytical models for the design of basal reinforced piled embankments

S.J.M. van Eekelen [a, b, *], A. Bezuijen [c, a], A.F. van Tol [a, b]

[a] Deltares, Unit Geo-Engineering, P.O. Box 177, 2600 MH, Delft, Netherlands
[b] Delft University of Technology, Netherlands
[c] Ghent University, Belgium

ARTICLE INFO

Article history:
Received 20 May 2014
Received in revised form
21 August 2014
Accepted 25 October 2014
Available online 20 November 2014

Keywords:
Geosynthetics
Piled embankments
Load transfer platforms
Geosynthetic reinforcement
Field monitoring
Arching

ABSTRACT

Van Eekelen et al. (2012a,b, 2013) have introduced an analytical model for the design of the geosynthetic reinforcement (GR) in a piled embankment. This paper further validates this model with measurements from seven full-scale tests and four series of scaled model experiments. Most of these measurements have been reported earlier in the literature.

The new model describes arching with the "Concentric Arching model" (CA model). This model is an extension of the single arch model of Hewlett and Randolph (1988) and the multi-scale model of Zaeske (2001), which is also described in Kempfert et al. (2004). For load-deflection behaviour, Van Eekelen et al. (2012a,b, 2013) proposed the use of a net load distribution that is inverse triangular instead of uniform or triangular. These authors also proposed the inclusion of all the subsoil support beneath the GR in the calculations.

On the basis of comparisons between the measurements and calculations, it is concluded that the CA model matches the measurements better than the models of Zaeske or Hewlett and Randolph.

Where there is no subsoil support, or almost no subsoil support, the inverse triangular load distribution on the GR strips between adjacent piles gives the best match with the measurements. Cases with subsoil support generally lead to less GR strain. In the cases with significant subsoil support, the load distribution is approximately uniform. In the cases with limited subsoil support, it should be determined which load distribution gives the minimum GR strain to find the best match with the measurements.

1. Introduction

Basal reinforced piled embankments are increasingly popular due to the good performance of these structures, mainly in areas with soft soil. They can be constructed quickly, they do not exert horizontal soil pressure on adjacent sensitive structures and residual settlement is very limited or absent. As a result, they require very limited maintenance. Several design guidelines have been published or updated lately in Europe, including the German EBGEO (2010), the Dutch CUR226 (2010, described in Van Eekelen et al., 2010b), the British BS8006 (2010, described and analysed in Van Eekelen et al., 2011) and the French ASIRI (2012). The CUR226 committee is currently working on an update to bring the CUR226 in line with recent research results. This paper presents a validation study that has been carried out to support the choices made for the update of CUR 226 (2015).

Analytical design models for the design of the basal reinforcement in piled embankments include two calculation steps. The first step calculates the arching behaviour in the fill. This step divides the total vertical load into two parts: load part *A*, and the 'residual load' ($B + C$ in Fig. 1). Load part *A*, which is also referred to as 'arching *A*', is the part of the load that is transferred to the piles directly.

The second calculation step describes the load-deflection behaviour of the geosynthetic reinforcement (GR, see Fig. 1). In this calculation step, the 'residual load' is applied to the GR strip between each pair of adjacent piles and the GR strain is calculated. The GR strip may or may not be supported by the subsoil, depending on the local circumstances.

An implicit result of step 2 is that the 'residual load' is divided into a load part *B*, which passes through the GR to the piles, and a load part *C*, resting on the subsoil, as indicated in Fig. 1.

* Corresponding author. Deltares, Unit Geo-Engineering, P.O. Box 177, 2600 MH, Delft, Netherlands. Tel.: +31 88 335 72 87.
E-mail address: suzanne.vaneekelen@deltares.nl (S.J.M. van Eekelen).

http://dx.doi.org/10.1016/j.geotexmem.2014.10.002

Glossary of terms

A, kN/pile	Load part transferred directly to the pile ('arching *A*' in this paper) expressed as kN/pile = kN/unit cell
a, m	Width of square pile cap
a_{eq}, m	Equivalent width of circular pile cap
all	Support of subsoil underneath *all* GR between the pile caps
B, kN/pile	Load part that passes through the geosynthetic reinforcement (GR) to the pile expressed as kN/pile = kN/unit cell
CA	Concentric Arches Model (Van Eekelen et al., 2013)
C, kN/pile	Load part that is carried by the soft soil between the piles (this soft soil foundation is referred to as the 'subsoil' in this paper) expressed as kN/pile = kN/unit cell
c, kPa	cohesion
d, m	Diameter circular pile (cap)
DEM	Discrete Element Method
E, kPa	Young's modulus
GR	Geosynthetic reinforcement
H, m	Height of the fill above the pile or pile cap
inv	Inverse triangular load distribution (see Fig. 3c)
J_x, J_y, kN/m	Tensile stiffness of the GR parallel to the road axis (x) or perpendicular to the road axis (y).
k, kN/m^3	Subgrade reaction
MD	Machine direction of a GR (the long direction)
p, kN/m^2	Uniformly distributed surcharge on top of the fill (top load)
PET	Polyester
PP	Polypropylene
PVA	Polyvinyl Alcohol
str	*Str*ip: support of subsoil underneath the GR *str*ips between adjacent pile caps only
s_x, s_y, m	Pile spacing parallel to the road axis (x) or perpendicular to the road axis (y).
t, m	Thickness of a soft soil layer underneath the embankment
tri	*Tri*angular load distribution (see Fig. 3a)
uni	*Uni*form load distribution (see Fig. 3b)
XMD	Direction perpendicular to the machine direction of a GR
Z	Multi-scale arching model of Zaeske (2001)
γ, kN/m^3	Fill unit weight
φ	Internal friction angle
ψ	Dilation angle
600/50, kN/m and kN/m	Indicates the strength of geosynthetic reinforcement layer. The first value (600 kN/m in this case) gives the characteristic short-term tensile strength in machine direction (MD) and the second value (50 kN/m in this case) gives the characteristic short-term tensile strength in the direction perpendicular to the machine direction (XMD).

Several analytical models have been proposed in the literature to calculate the first calculation step, the arching. They are listed and explained in Van Eekelen et al. (2013). They include frictional models, rigid arch models, models using mechanical elements and limit equilibrium models. The frictional models, which are based on Terzaghi (1943), include McKelvey (1994), Russell and Pierpoint (1997), McGuire et al. (2012), Naughton (2007) and Britton and Naughton (2008) and the model of Marston and Anderson (1913), which was modified by Jones et al. (1990) and adopted in the British Standard BS8006 (2010). The rigid arch models include Scandinavian models such as Carlsson (1987), Rogbeck et al. (1998, modified by Van Eekelen et al., 2003), Svanø et al. (2000), the enhanced arch model described in, for example, Collin (2004), the design method of the Public Work Research Center in Japan (2000, discussed in Eskişar et al., 2012). The models that consider the behaviour of the separate mechanical elements and match their boundaries are described in, for example, Filz et al. (2012), Deb (2010), Deb and Mohapatra (2013) and Zhang et al. (2012). The present paper focuses on the last family of arching models: limit equilibrium models. The following section describes these models.

Several approaches for the second calculation step have also been presented in the literature. The German approach (adopted in EBGEO, 2010; CUR 226, 2010), including some variations, is described in the following section. An approach using finite differences and minimisation of the total energy has been presented

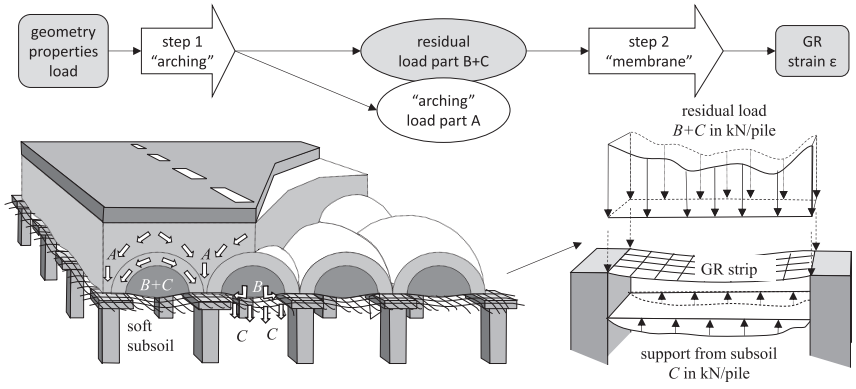

Fig. 1. Calculating the geosynthetic reinforcement (GR) strain comprises two calculation steps.

by Jones et al. (2010) with a 3D plate model, Halvordson et al. (2010) with a 3D cable-net model and Plaut and Filz (2010) with an axisymmetric model.

This paper validates three variations of limit equilibrium models for the arching of step 1 in combination with several variations of load-deflection membrane theory for step 2. Results obtained with the combination of these models are compared with measurements in seven full-scale cases and four series of scaled model experiments.

This paper specifically considers piled embankments with GR. Any reported measurements without GR were therefore not suitable for this paper. Examples are Hong et al. (2014) with 2D full scale experiments, Ellis and Aslam (2009a,b) and Lally and Naughton (2012) with centrifuge tests, Britton and Naughton (2008, 2010) with model experiments, and Hewlett and Randolph (1988) with scaled 2D trapdoor experiments.

Specific measurements are necessary to validate steps 1 and 2 separately. To validate step 1 separately, arching A needs to be measured. When GR is present, this needs to be measured above the GR. To validate a step 2 model, both arching A and the GR strain ε need to be measured. Only a very limited number of researchers have reported measurements of A in full-scale tests with GR (Van Eekelen et al., 2010a, 2012c; Van Duijnen et al., 2010) or scaled experiments with GR (Oh and Shin, 2007; Van Eekelen et al., 2012a). Van Eekelen et al. (2012b, 2013) and Van Eekelen and Bezuijen (2013) used most of these measurements to validate their proposed steps 1 and 2 separately.

When validating steps 1 and 2 together, measurements of A are not necessary and measurements of the GR strain suffice. Seven full-scale cases have been reported with the data that will be considered in the present paper: in Brazil (Spotti, 2006; Almeida et al., 2007, 2008), in Houten, the Netherlands (Van Duijnen et al., 2010), near Woerden, the Netherlands (Van Eekelen et al. 2012c), in Finland (Huang et al., 2009, including DEM calculations), in the Krimpenerwaard, the Netherlands (Haring et al., 2008), in Hamburg, Germany (Weihrauch et al., 2013) and in France (Briançon and Simon, 2012). Additionally, four series of model experiments reported in the literature are considered in the present paper: from Virginia (Sloan, 2011; McGuire et al., 2012), the Republic of Korea (Oh and Shin, 2007), Germany (Zaeske, 2001; also reported in Kempfert et al., 2004) and the Netherlands (Van Eekelen et al., 2012a,b).

Several other measurements reported in the literature were not suitable for use in the present paper because GR strains were not measured or not reported. They include Chen et al. (2008), Blanc et al. (2013, 2014) and Van Eekelen et al. (2010a). Zhuang et al. (2014) used this last reference for the validation of their simplified model, and calculated the 'measured' GR deflection from the measured load distribution.

Section 2 summarises the analytical models included for consideration. Section 3 includes a summary of the cases considered. Special attention is paid to the determination of the calculation parameters for each case. Section 4 compares the analytical calculation results with the measurements for each of the considered cases. Section 5 discusses the results.

2. Description of the considered analytical models

This paper validates several combinations of analytical models for step 1, the arching and step 2, the load-deflection behaviour. See Fig. 1 and Table 13.

2.1. Step 1: arching

The two most frequently used arching models in Europe are Hewlett and Randolph's single arch model (1988, see Fig. 2a) and Zaeske's multi-scale model (2001, also cited in Kempfert et al., 2004, see Fig. 2b). An extension of these two models is the Concentric Arches model (CA model, see Fig. 2c) presented recently by Van Eekelen et al. (2013). This model was specifically developed in response to the observation that a major part of the load on the GR concentrates on the GR strips between adjacent piles, and that the load distribution on these strips approaches the inverse triangular shape, as shown in Fig. 3c. This is further discussed in the next section.

The applicability of arching models should be limited to situations where the distance between the piles is comparable to those applied in the considered cases. When the distance between the pile caps becomes too large, the arching or rather 'punching' here is less efficient, as shown by Hong et al. (2014).

2.2. Step 2: load deflection behaviour

In the second calculation step, the 'residual load' that results from step 1 is applied to the GR strip between each two adjacent piles. The GR strip may be supported by subsoil. The GR strain is then calculated using differential equations based on membrane theory, as explained in Van Eekelen et al. (2012b).

Two issues are of major importance in step 2. Firstly, the load distribution on the GR strip has a strong influence on the calculated GR strain (see Fig. 3). Van Eekelen et al. (2012a,b, also discussed in Filz and Sloan, 2013) concluded that this distribution approaches the inverse triangular distribution as opposed to the triangular distribution of EBGEO (2010); CUR (2010) and Zaeske (2001) and the uniform distribution of BS8006 (2010). This is also confirmed by the findings of, for example, Han and Gabr (2002). These three load distributions are all considered in the present paper.

Secondly, subsoil support has a major influence. The most extreme situations occur when the subsoil support is lost. This can happen, for example, due to lowering the water table in the subsoil, the settlement of soft subsoil under the weight of a working platform below the GR, or migrating voids, for example due to old mine workings. To stay on the safe side in design, BS8006 disregards subsoil support.

Some design guidelines, such as EBGEO (2010) and CUR (2010), accept taking subsoil support into account. However, they only consider the subsoil beneath the GR strip under consideration between adjacent piles. Lodder et al. (2012) and Van Eekelen et al. (2012b) suggested using a modified value for the subgrade reaction k to take into account all subsoil underneath the entire GR. This suggestion is in line with the work of Jones et al. (2010), Halvordson et al. (2010), Plaut and Filz (2010) and Filz et al. (2012).

2.3. Validation of arching, load distribution on the GR and effect of subsoil support

Van Eekelen et al. (2013) recommend using the CA model, an inverse triangular load distribution and taking into account all soil support underneath the GR between the piles. They validated the CA model with laboratory experiments, numerical calculations of Le Hello and Villard (2009) and measurements in two full-scale cases (Van Eekelen et al., 2012c and Van Duijnen et al., 2010). Van Eekelen et al. (2012b) validated the inverse triangular load distribution with or without subsoil support with model experiments.

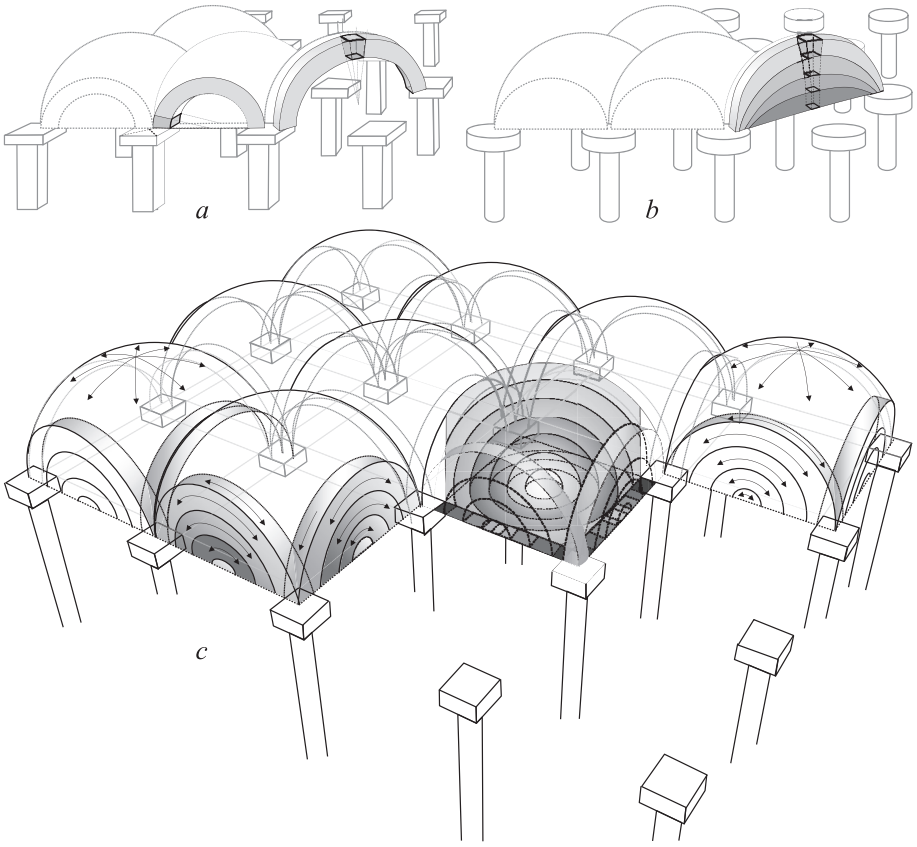

Fig. 2. Models for calculation step 1: arching, see Fig. 1. (a) Hewlett and Randolph's single arch model (1988), (b) Zaeske's multi-scale model (2001, also described in Kempfert et al., 2004, adopted in EBGEO, 2010; CUR 226, 2010) and (c) the Concentric Arches model (CA model, Van Eekelen et al. (2013).

The present paper gives additional validations for the variations in steps 1 and 2 described in the previous sections.

3. Case study descriptions

3.1. Introduction

This section briefly describes seven full-scale cases and four series of model experiments. Mean (best-guess) values for the parameters used in the calculations are determined. Characteristic values, which are the values generally used in design, cannot be used here.

The analytical models considered have been developed for cohesion-less frictional fills. In practice, however, fills often have some level of cohesion. For design purposes, it is advisable to disregard this cohesion. This simplification results in a 'safe' design: greater GR strain will be calculated than if cohesion is taken into account.

For the purposes of validation, however, cohesive fill is less suitable. It is possible to take cohesion into account by increasing the friction angle. However, for small stresses, the maximum difference between the two principal stresses is much larger for cohesive fills than for a fill with an artificially high friction angle. This means that higher tangential stresses can develop in a highly cohesive fill. This can result in a lot of arching and therefore low GR strains that are lower than any calculated GR strain with an artificially high friction angle. This paper focuses exclusively on piled embankments with frictional fills.

The subgrade reaction coefficient k (kN/m^3) was determined as follows, in order of preference:

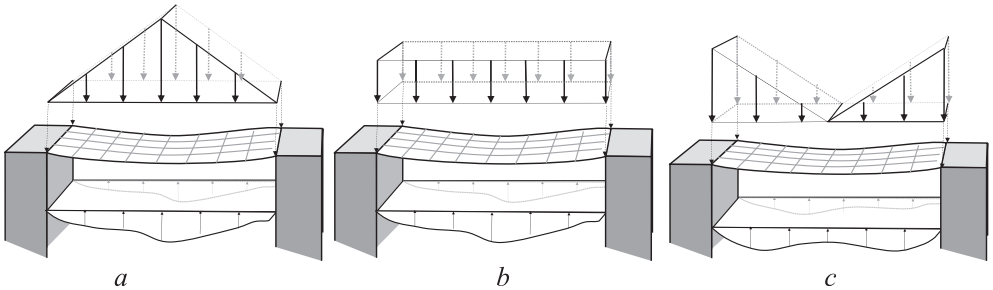

Fig. 3. Calculation step 2 with three different load distributions: (a) triangular (Zaeske, 2001; EBGEO, 2010; CUR, 2010) (b) uniform (BS8006, 2010) (c) inverse triangular (Van Eekelen et al., 2012a,b).

- In some cases the relationship between the vertical pressure p and settlement z is known, for example for an adjacent unreinforced area subjected to the same surcharge load. In those cases the value of k was determined using the relationship $k = p/z$. However, if the settlement measured in the adjacent field is much larger than the settlement in the piled embankment, the value selected for k should be lower. For example, in the case of Woerden (Section 3.3.1), it is expected that the weight of the working platform below the GR will have caused so much settlement that the contact between the subsoil and the GR will be lost, resulting in $k = 0$ kN/m^3. In other cases, subsoil support decreases when the contact between the GR and the subsoil is reduced during subsoil settlement.
- In some cases calculations were carried out using a simple 1D consolidation model. In those cases, the soil profile and the required soil parameters were determined with the results of the original soil investigation.
- In other cases, the Young's modulus E of the subsoil in combination with the thickness of the soft soil layer t or layers t_i is known. In those cases the value of k was determined using the relationships given in EBGEO (2010): $k = E/t$, or in the case of multiple layers: $k = E_1 \cdot E_2/(E_1 \cdot t_2 + E_2 \cdot t_1)$. It is possible that this leads to an underestimation of the subgrade soil reaction because the stiffness of the subsoil can increase due to the preloading caused by the pile installation or due to the negative friction along the pile shafts. Given this negative friction, it is not advisable to calculate k using large thicknesses for soft soils.

The installation of piles in soft soil results in (1) an increase in soft soil stiffness due to increasing stress and (2) negative friction along the pile shafts resulting in an apparent increase of stiffness. These effects are disregarded in the present paper.

A limitation of the study in this paper is that most field tests and numerical calculations did not continue until failure occurred and so no information is available about the ultimate limit state. However, model experiments by Zaeske (2001, section 3.11 and 4.11) and Van Eekelen et al. (2012a, see section 3.12 and 4.12) did continue in many cases until failure occurred. Furthermore, the authors of the present paper believe that the available data for the working condition are sufficient to determine the reliability of the analytical models for the working condition.

3.2. Full-scale test in Rio de Janeiro (Almeida et al., 2007, 2008)

Almeida et al. (2007, 2008) present measurements in a full-scale experiment carried out in the Barra da Tijuca District of Rio de Janeiro. The project has also been described in Spotti (2006), McGuire et al. (2009), Van Eekelen et al. (2014) and Zhuang et al. (2014). Part of the test area is shown in Fig. 4.

The embankment is relatively thin: at the test location, the average $H = 1.25$ m and so $H/(\sqrt{2}\cdot(s_x\text{-}a)) = 0.52$. This value is less than the minimum values allowed in the EBGEO (0.80) or CUR (0.66) for the usability phase. However, the low height is interesting for the construction phase and for research purposes.

A 1.0 m deep excavation was made before GR installation, as indicated in Fig. 4. The GR was kept taut by loading the edges with fill. Photos taken at the site show that the geogrid was indeed relatively taut but that some parts of the reinforcement did sag a little prior to placement of the fill. Compaction of the lower fill layers was carried out with care using light equipment.

A single layer of knitted Fortrac PET biaxial geogrid 200/200 was placed over the pile caps with an underlying layer of non-woven geotextile to reduce abrasion between the pile cap and the geogrid. The failure strain of PET geogrids is around 10%. The fill material consisted of a clayey sand compacted to at least 95% of the standard Proctor maximum. It has a compacted unit weight $\gamma = 18.0$ kN/m^3. Adjacent geogrids were joined together by seaming.

The GR deflection was measured with settlement plates (SP) installed at the GR level at the locations indicated in Fig. 4. GR strain gauges (ε in Fig. 4) consisted of an ingenious system described by Almeida et al. (2007) which measured the strain using strain gauges on a steel bar that had been attached with a reaction spring to the GR.

3.2.1. Determination of parameters

The stiffness J (kN/m) of the geogrid depends on the tensile force and the loading time. The average of the larger values for the measured GR strains is 1.5% (see Fig. 15). The total loading time is

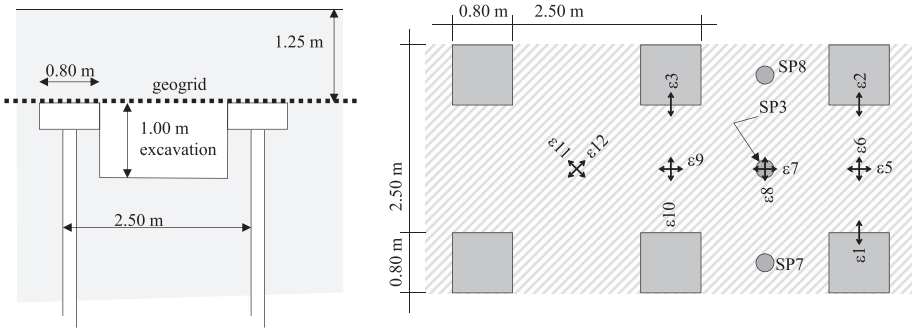

Fig. 4. Layout of the part of the experimental site under consideration in the Barra da Tijuca District, Brazil Drawing modified after Spotti (2006) and Almeida et al. (2007). The shaded area was excavated prior to the installation of the reinforced embankment.

Table 1
Parameters used in the calculations of case Almeida et al. (2007, 2008).

Centre-to-centre distance piles $s_x = s_y$ m	Width square pile caps a m	Height fill H m	unit weight fill γ kN/m^3	Friction angle fill φ deg	Subgrade reaction k kN/m^3	Stiffness GR $J_x = J_y$ kN/m	Surcharge load p kPa
2.50	0.80	1.25	18.0	43–68[a]	0	1615	0

[a] In the comparison in Section 4.2, the value of φ has been varied. In section 5, $\varphi = 68°$ has been used because this value gives the lowest GR strains of the two possibilities given in this section.

188 days. The isochronous curves of the applied geogrid give $J_{1.5\%,1\ month} = 1637$ kN/m and the $J_{1.5\%,1\ year} = 1594$ kN/m. We assume that the average of these values is $J_{1.5\%,188\ days} = 1615$ kN/m.

Direct shear tests on fill samples given in Spotti (2006) show an average friction angle $\varphi = 42^\circ$ and an average cohesion $c = 18.9$ kPa. As described in Section 3.1, the high cohesion value results in a limitation for validation purposes. However, it was believed worthwhile to include this case in this study because of the excavation below the GR and the low embankment. It was therefore necessary to find an equivalent friction angle φ for $c = 0$. An equivalent φ can be found by determining the fill strength at the average pressure at GR level ($\sigma_v = \gamma \cdot H + p = 18 \cdot 1.25 = 22.5\ kPa$). From this, it follows that:

$$\varphi_{virtual;c=0} = atan\left(\frac{\sigma_v tan\varphi + c}{\sigma_v}\right) = atan\left(\frac{22.5 * tan42^o + 18.9}{22.5}\right) = 60^o \quad (1)$$

However, McGuire et al. (2009) have found (after back-calculations from measurements in nearby 2D test fields): $\varphi = 68^\circ$ for $c = 0$ kPa. McGuire et al. consider these results satisfying, although their value for φ seems unreasonably high.

To prevent misinterpretation as a result of selecting the wrong friction angle, a wide range of values for φ was used in the calculations of this paper. Table 1 summarises the parameters used in the calculations.

3.3. Full-scale case in Woerden (Van Eekelen et al., 2012c)

A motorway exit was rebuilt near Woerden, a city in the centre of the Netherlands. The work involved building a new road on a piled embankment. Van Eekelen et al. (2012c, 2015) reported monitoring results from this project.

The part of the test area considered in this paper is shown in Fig. 5. The subsoil consists of 17 m of very soft clay. Over 900 precast square pile caps were placed on precast driven piles. The amount of arching was measured with total pressure cells on top of pile caps 692 and 693, above the GR. These pile caps were accordingly replaced by circular pile caps with the same area as the square ones. The pressure cells had the same diameter as the circular pile caps.

The embankment fill consisted of 0.18 m asphalt, 0.25 m asphalt gravel mixture and, below that, a fill of crushed recycled construction material, mainly concrete. The distance between asphalt surface and pile cap ranges from 2.11 m above pile cap 691 and 1.70 m above pile cap 682.

In the transverse direction, a layer of knitted PET geogrid reinforcement Fortrac 600/50 was installed with an underlying layer of 0.05–0.16 m of sand to protect the reinforcement. A second layer of the same material was installed on top of and perpendicular to the first layer. The failure strain of PET geogrids and PET geotextiles is around 10%.

The GR strains were measured with optic fibres at the locations "ε" in Fig. 5. Additionally, the GR strains were measured at three locations elsewhere in this piled embankment with a system of steel cables, as explained in Van Eekelen et al. (2012c). The GR strains measured with the last system were 0.2% during the first six weeks. As the optic fibres started measuring after these six weeks, the initial 0.2% GR cable strain was added to the optic-fibre measurements, as shown later in Section 4.3 of this paper. The resulting GR strains correspond to the GR deflection measured with a liquid levelling system in tubes.

The new exit went operational in June 2010. The present paper reports the average strains measured during six weeks in August and September 2013, in other words 38 months after the road was opened.

3.3.1. Determination of parameters

The friction angle of the fill of compacted crushed recycled material is assumed to be around 51°. This value is based on large triaxial tests on similar material by both Den Boogert et al, (2012) and Van Niekerk et al. (2002).

The stiffness of the GR layers in both directions can be summed, as shown by Van Eekelen and Bezuijen (2014). In each direction 600 + 50 = 650 knitted PET geogrid was installed. It has, at small strains (less than 1.5%) and with a loading time of three years, a tensile stiffness of ca. 4936 kN/m. This value was determined with the isochronous curves provided by the GR supplier.

Before the installation of the piles, a working platform was installed on the soft subsoil. The working platform consisted of 0.75 m of sand. The working platform was left underneath the GR and caused subsoil settlement.

This settlement of the subsoil underneath the GR caused by the weight of 0.75 m of sand was predicted using a simple 1D consolidation model based on CPT and triaxial test results. The calculations resulted in values for subsoil settlement that were well in excess of the 0.11 m measured after the road went operational.

It is therefore concluded that the subgrade reaction k must have reached a minimum and is approximately 0 kN/m^3. This value is given in Table 2, along with the other properties and the geometry used in the calculations.

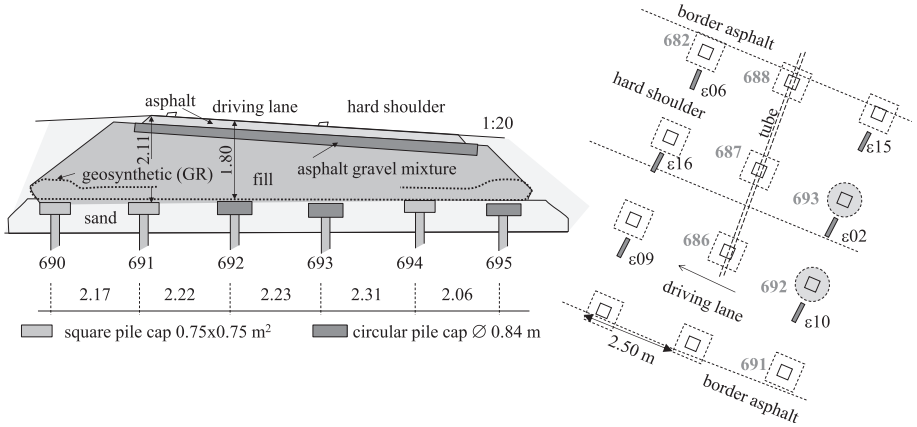

Fig. 5. Layout of the part of the monitored site under consideration in Woerden, the Netherlands, including the instrumentation relevant for the present paper (Van Eekelen et al., 2012c).

Table 2
Parameters used in the calculations for Woerden (Van Eekelen et al., 2012c).

Centre-to-centre distance piles $s_x = s_y$ m	Width square pile caps a m	Height fill H m	unit weight fill γ kN/m^3	Friction angle fill φ deg	Subgrade reaction k kN/m^3	Stiffness GR $J_x = J_y$ kN/m	Surcharge load p kPa
2.25	0.75	1.79	18.3	51	0	4936	0

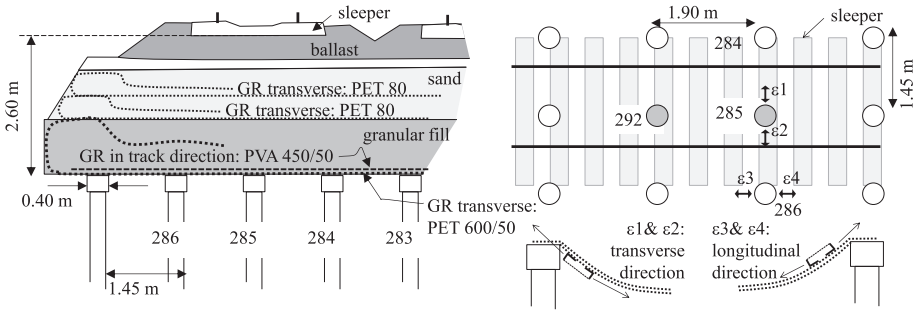

Fig. 6. Layout of the part of the monitored site under consideration in Houten, the Netherlands. Drawing modified after Van Duijnen et al. (2010). Detail in bottom right-hand corner: location of strain gauges.

3.4. Full-scale case in Houten (Van Duijnen et al., 2010)

Van Duijnen et al. (2010) and Van Duijnen (2014) presented monitoring results from a railway widening project described by Van der Stoel et al. (2010). The railway is located in Houten, the Netherlands. Fig. 6 shows the test area that is considered in this paper. The subsoil consists (top-down) of 1 m of sand, 3 m of soft clay and 20 m of sand. The piles and pile caps are cast in situ. The embankment fill consisted (top-down) of 0.4 m of ballast of crushed stones below the sleepers, 0.1 m blinding layer, 1.0 m of sand and 1.0 m of crushed granular fill (recycled construction material, mainly concrete).

Three layers of Fortrac reinforcement were installed in the transverse direction. The basal layer is a knitted PET geogrid 600/50 installed upon the pile caps with an underlying layer of sand to protect the reinforcement. Higher in the fill, two layers of knitted PET geogrid 80 were installed, as indicated in Fig. 6. In the direction of the track, a layer of knitted PVA geogrid 450/50 was installed on top of the basal GR layer. The failure strain of PET geogrids is around 10%, the failure strain of PVA geogrids is around 5%. The arching in the embankment was measured with total pressure cells on top of piles 285 and 292, above the GR layer, with the same diameter as the pile caps. Other measurements have been reported by Van Duijnen et al. (2010).

GR strains in the basal reinforcement layer were measured with Glötzl strain gauges at the locations "εx" in Fig. 6. Strain gauges ε1 and ε2 measure the strains in the transverse direction and they were installed below the bottom GR layer. Strain gauges ε3 and ε4 measure the strain in the direction of the track and they were installed on top of the longitudinal (in other words, in the direction of the track) GR layer. As shown in the picture at the bottom right-hand side of Fig. 6, it is expected that strain gauges ε1 and ε2 could result in a higher GR strain than the real GR strain due to the curvature of the deflected GR. Strain gauges ε3 and ε4, however, might measure a smaller strain than the real GR strain due to the bending.

The railway went operational in November 2008. This paper reports the average of the strains measured in 2010.

3.4.1. Determination of parameters

The fill material consists of different layers, as indicated in Fig. 6. It is assumed that the bottom level is decisive for the arching. This layer is comparable to the fill in Woerden and its friction angle is also assumed to be around 51°, as explained in section 3.3.

The stiffness of the reinforcement was determined as follows. In the longitudinal direction, the total reinforcement consists of woven PVA geogrid 450 + woven PET geogrid 50. The stiffness of the separate layers may be summed, as described in Van Eekelen and Bezuijen (2014). At a maximum 1.5% strain and a loading time of two years, this gives a tensile stiffness $J_{along} = 5237$ kN/m. In the transverse direction, the two upper layers were installed quite a large distance above the pile caps and it is therefore assumed that it is not correct to add their stiffness to the total stiffness. The total reinforcement is therefore woven PET geogrid 600 + woven PVA geogrid 50. At small strains (max 1.5%) and a loading time of two years, this gives a tensile stiffness $J_{across} = 5208$ kN/m. These values were determined with the isochronous curves provided by the GR supplier.

The subgrade reaction k was calculated using natural strain and consolidation based on correlations to derive the parameters from CPTs and triaxial tests. Later, settlement measurements became available for a nearby embankment on the same subsoil. It was concluded that the measured settlement was 30% less than predicted. The subgrade reaction was therefore divided by 0.7 to obtain a more realistic value. The resulting value is given in Table 3, along with the other properties and the geometry used in the calculations.

3.5. Large-scale French experiments (Briançon and Simon, 2012; Nunez et al., 2013)

Briançon and Simon (2012) and, for example, Nunez et al. (2013) reported a series of large-scale tests. The researchers carried out

Table 3
Parameters used in the calculations for Houten (Van Duijnen et al., 2010).

Centre-to-centre distance piles s_x along m	Centre-to-centre distance piles s_y across m	Diameter circular pile caps d m	Height fill H m	unit weight fill γ kN/m^3	Friction angle fill φ deg	Subgrade reaction k kN/m^3	Stiffness GR along J_x kN/m	Stiffness GR across J_y kN/m	Surcharge load p kPa
1.90	1.45	0.40	2.60	18.3	51	480	5237	5208	0

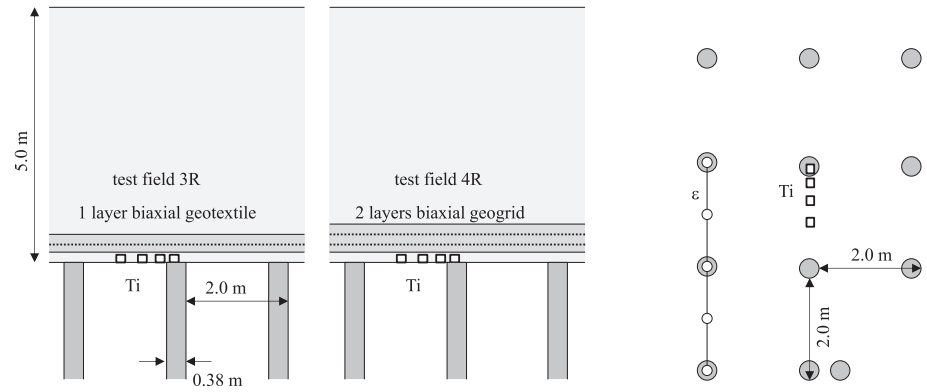

Fig. 7. Layout of the part of fields 3R and 4R under consideration in the large-scale tests in France with settlement transducers Ti. Drawing modified after Briançon and Simon (2012).

tests in four test fields. Two of them are considered in this paper: test fields 3R and 4R. The researchers placed 8 x 4 circular concrete piles in a square arrangement in each test field, as indicated in Fig. 7. No pile caps were installed.

The load transfer platform in test field 3R consisted of (bottom-up) a 0.15 m working platform, 0.2 m of industrial gravel (0–31.5 mm), a layer of biaxial PET geotextile and 0.2 m of industrial gravel. The failure strain of PET geotextiles is around 10%. The industrial gravel consisted of crushed recycled road construction material.

The load transfer platform of test field 4R consisted of (bottom-up) a 0.15 m working platform, 0.2 m of industrial gravel (0–31.5 mm), a layer of biaxial geogrid, 0.2 m of industrial gravel, another biaxial geogrid and 0.1 m of industrial gravel. At the embankment edges, the GR was wrapped around and anchored back into the embankment.

The rest of the embankment was a marly and chalky natural soil. The total height of the embankment was 5.0 m. Settlement was measured at locations Ti in Fig. 7. Optic fibres (Geodetect® strips) were used to measure GR strains in field 3R, as indicated with ε in Fig. 7.

3.5.1. Determination of parameters

In one of the neighbouring test fields, no GR or piles were applied. The weight of the embankment was 92.5 kPa. An average maximum settlement of 0.26 m was measured at the original ground level after 165 days. The subgrade reaction k is therefore $92.5/0.26 = 356$ kN/m^3. The subsoil therefore provides considerable support.

Briançon and Simon (2012) give a friction angle $\varphi = 36°$ and an effective cohesion c = 60 kPa for the fill of industrial gravel. As described in section 3.2, a cohesive fill is less suitable for comparing measurements with analytical models not meant for cohesive material.

An equivalent φ can be found by determining the fill strength at the average pressure at GR level ($\sigma_v = \gamma \cdot H + p = 20 \cdot 5 + 0 = 100\ kPa$). From this, it follows that:

$$\varphi_{virtual;c=0} = atan\left(\frac{\sigma_v tan\varphi + c}{\sigma_v}\right) = atan\left(\frac{100 * tan36^o + 60}{100}\right) = 53^o \quad (2)$$

In their Table 3, Briançon and Simon (2012) give the results of EN ISO 10319 tensile tests on the GR. The short-term tensile stiffness for 2% GR strain was determined at 800 kN/m for test field 3D and 500 kN/m per GR layer for test field 4R. The measurements in the test field were carried out over a period of approximately six months. The stiffness of the GR was therefore reduced by 25% in a loading time of six months, which is a normal reduction for PET for this loading period. The resulting values are listed in Table 4.

3.6. Full-scale test and 2D DEM calculations of Huang et al. (2009)

A geosynthetic reinforced embankment was constructed on deep mixing (DM) columns and DM walls for an approach to a new bridge over the Sipoo River in Hertsby, Finland. Forsman et al. (1999) and Forsman (2001) give detailed information about the project. Huang et al. (2009) presented monitoring results and compared the measurements with 2D DEM (Discrete Element Method) calculations.

Fig. 8 presents the test area. The subsoil consists of a crust of 1–1.5 m, 10–14 m of soft clay, 1–6 m of silt and 1–5 m of glacial till. Deep mixing (DM) columns with a diameter of 0.80 m were installed following the pattern shown in Fig. 8. Some of the DM columns were installed in such a way as to effectively create a wall. The average thickness of these DM walls was estimated to be 0.70 m. No pile caps were installed.

The embankment consisted (top-down) of 0.05 m of asphalt, a base course of 0.20 m of crushed stone, a sub-base of 1.05 m of gravel and a 0.50 m sand working platform above the existing ground.

A layer of woven biaxial geotextile 200/200 was installed with a 0.3 m thick underlying layer of sand to protect the reinforcement. Huang et al. (2009) did not specify the material used for the

Table 4
Parameters used in the calculations of the large-scale tests of Briançon and Simon (2012).

Test	Centre-to-centre distance piles s_x along = s_y across m	Diameter circular pile caps d m	Height fill H m	unit weight fill γ kN/m3	Friction angle fill φ deg	Subgrade reaction k kN/m3	Stiffness GR $J_x = J_y$ kN/m	Surcharge load p kPa
3R	2.00	0.38	5.00	20	40–78[a]	356	600	0
4R	2.00	0.38	5.00	20	40–78[a]	356	750	0

[a] In the comparison in Section 4.7, the value of φ has been varied. In Fig. 18 and Section 5, $\varphi = 53°$ has been used.

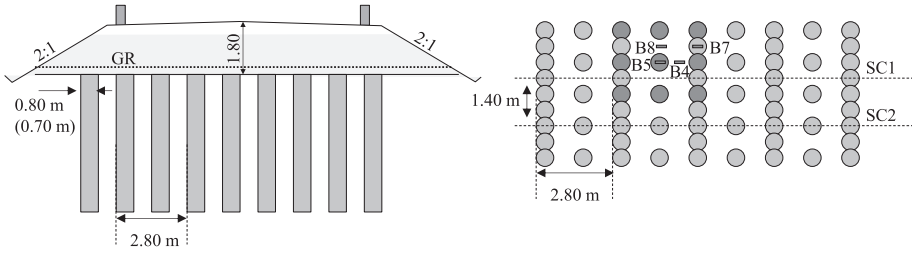

Fig. 8. Layout of the monitored site on DM columns in Hertsby, Finland. Drawing modified after Huang et al. (2009).

Table 5
Parameters used in the calculations to compare with Huang et al. (2009).

	Centre-to-centre distance DM piles/walls $s_x = s_y$ m	Width DM walls a/diameter columns d m	Height fill H m	Unit weight fill γ kN/m^3	Friction angle fill φ deg	Subgrade reaction k kN/m^3	Stiffness GR $J_x = J_y$ kN/m	Surcharge load p kPa
2D[a]	1.40	0.70	1.80	20	41.5	19.5	1700	12
3D	1.40	0.80	1.80	20	41.5	19.5	1700	12

[a] Plane strain.

reinforcement but they indicated the stiffness of the GR used in their 2D DEM calculations: $J = 1700$ kN/m.

GR strains were measured at the locations indicated in Fig. 8 (B4, B5, B7 and B8). The bridge approach was constructed in 1996 and 1997. This paper compares the GR strains measured during the first five years after putting the road into use.

Huang et al. (2009) simulated the project with 2D DEM calculations using FLAC. They used coupled mechanical and hydraulic modelling. This means that the pore water pressure changes and effective stress changes were calculated alternately in a continuous loop. To convert the 3D problem to a 2D one, they investigated two cases: (SC1) without mid-columns and (SC2) with mid-columns as indicated in Fig. 8.

This paper presents the following two analytical calculations: (1) a 2D calculation (with a 2D plane strain version of the CA model) like the SC2 of Huang et al. Accordingly, the walls have a centre-to-centre distance $s_x = 1.40$ m and a wall width of 0.70 m. It is expected that this calculation will result in smaller GR strains than measured. And (2) a fully 3D configuration, with only columns and no walls. This simulates the situation with only the dark-coloured columns in Fig. 8. The centre-to-centre distances are $s_x = s_y = 1.40$ m and the column diameter $d = 0.80$ m. It is expected that this calculation will result in slightly higher values for GR strain than measured.

Huang et al. (2009) included a traffic load as a uniformly distributed load of 12 kPa. This value was adopted for the calculations presented in the current paper.

3.6.1. Determination of parameters

Huang et al. (2009) give a friction angle $\varphi = 38^\circ$ and a cohesion $c = 5.0$ kPa. It is necessary to find an equivalent friction angle φ for $c = 0$ using the method given in Section 3.2.1:

$$\varphi_{virtual;c=0} = atan\left(\frac{\sigma_v tan\varphi + c}{\sigma_v}\right) = 41.5^o \quad (3)$$

The subgrade reaction k is calculated from the thickness of the soft soil layers in combination with the Young's modulus E of these layers. The 15 m thick layer of soft clay has an E of 300 kPa. The 2 m thick layer of silt has an E of 1600 kPa. The resulting subgrade reaction is: $k = (300 \cdot 1600)/(2 \cdot 300 + 15 \cdot 1600) = 19.5$ kN/m^3. Subsoil support in this case was therefore very limited. This value has been listed in Table 5, along with the other parameters.

3.7. The Krimpenerwaard piled embankment for the N210 road (Haring et al., 2008)

A new 14 km long regional road was built on a 15 m layer of extremely compressible organic soil. Haring et al. (2008) reported monitoring results from this project.

The part of the test area considered in this paper is shown in Fig. 9. The same precast square pile caps as in Woerden (see section 3.3) were installed on driven precast piles. The embankment fill consisted of 0.18 m of asphalt on top of an embankment of gravel consisting of crushed recycled construction material, mainly concrete. During the measurements, however, the asphalt had not yet been laid. An extra 0.18 m layer of gravel was placed to compensate for this.

The test field was established in 2007, which was during the optimisation process of the construction process. The space between the pile caps in the test field was not filled and the GR was installed on top of the pile caps with gaps in between. This construction method made it difficult to get the GR taut and so it was decided to fill the gaps between the pile caps with loose soil before

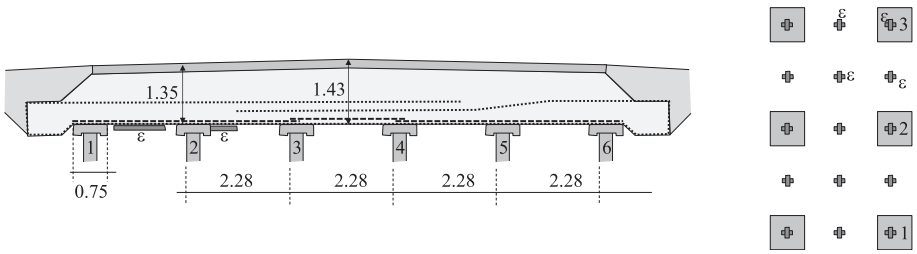

Fig. 9. Layout of the part of the monitored site under consideration in the N210 in the Krimpenerwaard, the Netherlands, indicating the location of the strain gauges applied for measuring GR strains Drawing modified after Haring et al. (2008).

Table 6
Parameters used in the calculations for the Krimpenerwaard N210 road (Haring et al., 2008).

	Centre-to-centre distance piles alongs_x m	Centre-to-centre distance piles acrosss_y m	Width square pile caps a m	Height fill H m	Unit weight fill γ kN/m^3	Friction angle fill φ deg	Subgrade reaction k kN/m^3	Stiffness GR alongJ_x kN/m	Stiffness GR acrossJ_y kN/m	Surcharge load p kPa
2 GR layers across	2.35	2.28	0.75	1.35	19.0	51	250	5178	5548	0
1 GR layer across[a]	2.35	2.28	0.75	1.35	19.0	51	250	5178	2959	0

[a] These cases are included in Fig. 27.

GR installation for the rest of the road. The problems with the GR installation in the test field may have resulted in unexplainable measurements. The road surface, however, has remained settlement-free during the first four years of using the road.

In the transverse direction, a layer of woven PET Stabilenka geotextile reinforcement 350/50 was installed with underlying pieces of non-woven on top of the pile caps to protect the reinforcement. This geotextile was wrapped back, as indicated in Fig. 9. This effectively results in two layers of cross-reinforcement. The reinforcement in the direction of the road consisted of knitted PET geogrid Fortrac 600/50. The failure strain of PET geogrids and PET geotextiles is around 10%. The GR strains were measured with Glötzl strain gauges at the locations "ε" in Fig. 9.

The new road was opened in 2010. This paper reports the average strains measured on 29 September 2007, which was 2 months after the building of the embankment but before the road went operational.

3.7.1. Determination of parameters

The fill material was comparable to the fill in Woerden and Houten (Sections 3.3 and 3.4) and its friction angle is also assumed to be around 51°, as explained in section 3.3.

The stiffness of the GR layers in both directions may be summed, as proposed by Van Eekelen and Bezuijen (2014). All the reinforcement consisted of knitted or woven PET. In the longitudinal direction, the short-term strength of this material is 600 + 50 + 50 = 700 kN/m. In the transverse direction, the short-term strength is 350 + 350 + 50 = 750 kN/m. The isochronous curves give, at 2.5% strain and a loading time of approximately 1 year, stiffness values J of 5178 kN/m and 5548 kN/m respectively for these materials. However, a better approach could be to disregard the upper GR layer since the distance between the bottom and top layers is considerable, as shown in Fig. 9. If the embankment is considered as a bending beam, the top layer cannot contribute much. In that case, the short-term strength will be 350 + 50 = 400 kN/m. This results in a stiffness J of 2959 kN/m. Both approaches will be considered.

The pressure on the subsoil below the GR is approximately 13.5 kPa. It is assumed that this pressure is the same for the entire area between the pile caps and it is therefore concluded that the subgrade reaction $k \cong 250$ kN/m^3. This was concluded from the pressure below the GR ≅ 13.5 kPa, which was measured at two locations: between two piles and four piles in combination with a measured GR deflection of 45–70 mm at these locations, which were averaged to assess the subgrade reaction. Table 6 gives the parameters used in the calculations of this case.

3.8. Hamburg full-scale test (Weihrauch et al., 2010, 2013)

The level of several streets in Hamburg's HafenCity is being raised by around 3 m to ensure safety from flooding. Weihrauch et al. (2010, 2013) reported measurements in a piled embankment constructed in the Hongkongstrasse. Vollmert (2014) supplied more data.

Part of the test area is presented in Fig. 10. Later, the right-hand part of the piled embankment was removed and a wall was installed as indicated. The subsoil consists of 15 m of layered soft soil. Top-down the layers consist of very loose sandy, partially clayey fills, clay-soft peaty clay, soft sandy clay, peat and sand. The average layer thickness of the organic layers is approximately 8.2 m. There were no significant differences between the geotechnical properties of the top fill layer and that of the original ground before filling up.

Unreinforced lime-cement treated gravel columns were installed at a centre-to-centre distance $s_{along} \times s_{across} = 2.50 \times 2.30$ m. The pile caps were widened with cast in situ unreinforced concrete to a diameter of 0.60 m.

The fill consists of a sand layer with a 0.30 m layer of asphalt and its foundation. In the direction perpendicular to the road axis, a laid Secugrid PET-200 geogrid layer was installed 0.15 m above the columns and wrapped back 0.25 higher in the fill across the entire road. In the longitudinal direction (along the road axis), a laid PET-400 geogrid layer of the same type was installed at 0.30 m above the columns. The failure strain of PET geogrids is around 10%. The GR strains were measured at the four locations indicated in Fig. 10.

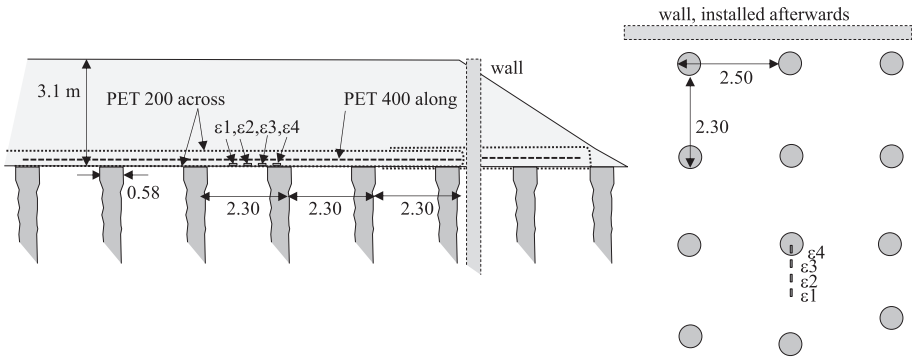

Fig. 10. Layout of the part of the test field under consideration in the Hongkongstrasse, Hamburg, Germany Drawing modified after Weihrauch et al. (2010, 2013).

Table 7
Parameters used in the calculations for Hamburg (Weihrauch et al., 2010, 2013).

	Centre-to-centre distance piles along s_x m	Centre-to-centre distance piles across s_y m	Diameter columns d m	Height fill H m	Unit weight fill γ kN/m^3	Friction angle fill φ deg	Subgrade reaction k kN/m^3	Stiffness GR $J_x = J_y$ kN/m	Surcharge load p kPa
During installation	2.50	2.30	0.58	2.50	19.0	35	1765	7480	18
Long term	2.50	2.30	0.58	3.10	19.0	35	1200	6050	20

Table 8
Parameters used in the calculations for the large-scale experiments of Sloan (2011).

Test	Centre-to-centre distance piles $s_{along} = s_{across}$ m	Diameter circular pile caps d m	Height fill H m	Unit weight fill γ kN/m3	Friction angle fill φ deg	Subgrade reaction k kN/m3	Stiffness GR along J_x kN/m	Stiffness GR across J_y kN/m	Surcharge load p kPa
CSE#3	1.83	0.61	1.86	22.00	45	0	493[a]	569[a]	0
CSE#4	1.83	0.61	2.29	21.53	45	0	493[a]	569[a]	0

[a] On the basis of the illustrations in Sloan (2011), it is assumed that the GR strain measurements were made in the transverse direction, and therefore that $J_x = 493$ kN/m.

3.8.1. Determination of parameters

The stiffness J (kN/m) of the geogrid was determined using the isochronous curves, the loading time and the measured GR strains. Table 7 gives the resulting GR stiffness, along with the other parameters provided by Vollmert (2014). He determined the subgrade reaction k with the measured GR deflection and the measured pressure beneath the GR.

3.9. Large-scale experiments (Sloan, 2011)

Sloan (2011, also reported in McGuire et al., 2012) carried out five large-scale tests. This paper considers two of the tests, namely CSE#3 and CSE#4 (Table 8). Nine circular ⌀ 0.61 m concrete columns were placed in a square arrangement within a square of concrete walls, as indicated in Fig. 11. The spaces between the box walls and piles were filled with a geofoam of expanded polystyrene (EPS) to model the soft subsoil between the piles. After installing a reinforced embankment on top of the columns and the EPS, the EPS was dissolved using D-limonene through a network of PVC pipes. D-limonene is a natural oil obtained from orange peels that dissolves EPS easily.

After dissolving the geofoam, the researchers waited 7 days and then loaded the embankment with a small working truck weighing 1878 kg with 4 wheels and measuring length × width = 3.0 × 1.4 m^2.

Three layers of biaxial punched/drawn Tensar® BS1500 geogrid of PP were installed. The authors of this paper did not have the failure strain for these PP geogrids at their disposal. One layer was placed directly on the columns. The other two GR layers were placed transversely with respect to each other at an elevation of 0.15 m above the first GR layer. GR strain measurements were made with wire extensometers, attached to the base layer of the GR. The locations of the GR strain transducers "ε" are indicated in Fig. 11. Transducers ε1, ε2 have been installed in test CSE#3 and ε3, ε4, ε5 in test CSE#4.

The fill consisted of gravel with 5% fines. This relatively low fines content was chosen to reduce the risk of an artificially high strength due to negative pore water pressure. The fill was compacted dry to avoid capillarity and increased strength due to negative pore water pressures.

3.9.1. Determination of parameters

Large GR strains were measured during the piled embankment tests. Sloan (2011, table 7.3) gives the rapid loading tensile stiffness of the reinforcement for several strains and states that stiffness falls by approximately 55% during the experiments. At 8% strain and a loading time of 7 days, this results in the following tensile stiffness: in machine direction (MD) 139 kN/m and in XMD direction 215 kN/m per layer. Consequently, the total stiffness in one direction (MD + MD + XMD) is 2·139 + 215 = 493 kN/m. In the other direction, the total stiffness is (XMD + XMD + MD) = 569 kN/m. It is possible that the reduction of the stiffness by 55% is not accurate as PP is a material that creeps considerably. The resulting values are stated in Table 8, along with the other geometry and material properties. The value for the fill friction angle was taken from Sloan (2011).

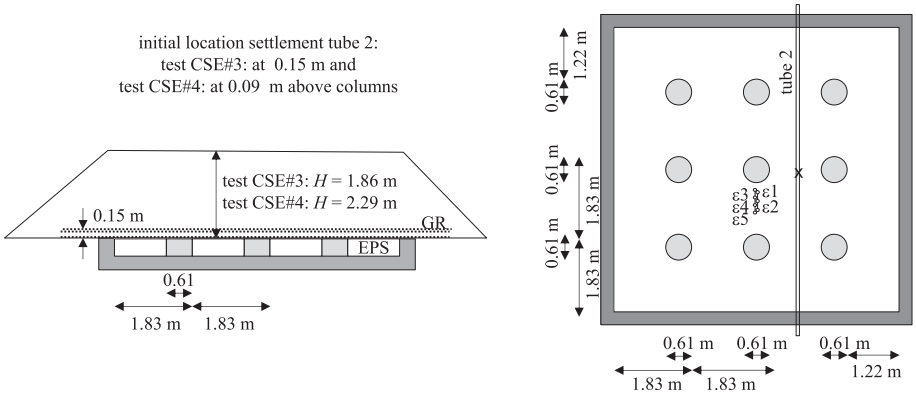

Fig. 11. Layout of large-scale tests CSE#3 and CSE#4 carried out in the USA (Sloan, 2011). Drawing modified after Sloan (2011).

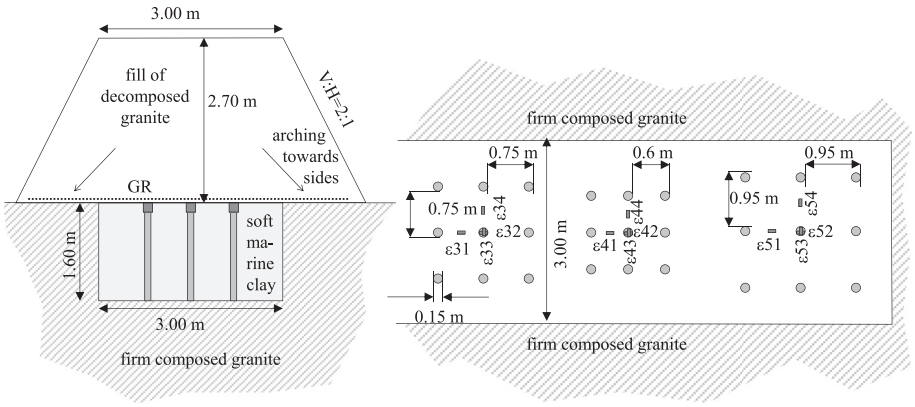

Fig. 12. Layout of the three test fields with piles and GR. Drawing modified after Oh and Shin (2007).

3.10. Oh and Shin's scaled tests (2007)

Scaled field experiments were performed at the Geotechnical Experimentation Site of the University of Incheon in the Republic of Korea (Oh and Shin, 2007). Fig. 12 presents part of the test area. A test box with length • width • depth = 13.0 m • 3.0 m • 1.6 m^3 was excavated in a firm composed granite and filled with marine clay obtained from the Bay of Incheon. After a consolidation period of 3 months, five test fields were installed, one with no piles or GR, one with only piles, and three with both piles and GR. In these three test fields, the centre-to-centre distance of the piles was 0.75, 0.60 and 0.95 m respectively. In each test field nine concrete piles with a diameter of 0.10 m were driven into the clay and a concrete pile cap with a diameter of 0.15 m was installed on each of the piles.

The embankment was built in three stages to heights of 0.67 m, 1.65 m and 2.70 m respectively. It consisted of a granite weathered soil, which is a poorly graded silty sand according to the authors.

A limitation of the structure is that arching occurs towards the sides of the test box, as indicated in Fig. 12. Oh and Shin (2007) indeed found, in their Fig. 13, that the total measured load was approximately 60% lower than the embankment weight.

A biaxial punched/drawn PP geogrid type Tensar® BS1100 was installed directly on top of the pile caps. The authors of this paper did not have the failure strain for these PP geogrids at their disposal. GR strains were measured with a plastic gauge (type YFLA-5) in both directions, both on top of a pile and mid-way between adjacent piles.

3.10.1. Determination of parameters

The value for the fill friction angle φ in Table 9 was taken from Oh and Shin's table 4 (2007). The cohesion given in this table is $c = 1.0$ kPa, which is considered negligible.

For the test field without piles or GR, Oh and Shin found, at $H = 1.65$ m, a maximum value for settlement of $z = 0.063$ m. These values are considered to be normative for the determination of the subgrade reaction k, as this settlement is comparable to the final settlement in the test fields with piles and GR for the embankment height of 2.70 m. At this embankment height, they also found arching towards the test box sides. The total measured load in the piled areas was more than 60% lower than expected. In this paper, it is assumed that the loss of load due to arching in the test field without piles is slightly less: 50%. This gives the subgrade reaction: $50\% \cdot \gamma \cdot H/z = 0.5 \cdot 18 \cdot 1.65/0.063 = 236$ kN/m^3.

The short-term stiffness at 2% GR strain was 205 kN/m in the machine direction and 330 kN/m in the transverse direction. A reduction of 12% in G R stiffness was applied to take into account the influence of the loading time. This reduction is confirmed by the measured development of the strain (Oh and Shin, their Fig. 15). Apparently, the subsoil support is enough to prevent continuous creep of the PP reinforcement. In the calculations, the average stiffness in both directions was used since the GR strains measured by Oh and Shin are probably the average of both directions. It should be noted that Oh and Shin simulated their tests with 2D plane strain FLAC calculations using $J = 800$ kN/m, despite their tensile test results.

3.11. Laboratory scaled experiments (Zaeske, 2001; Kempfert et al., 1999, 2004)

Zaeske (2001) and Kempfert et al. (1999, 2004) reported a series of scaled laboratory tests. Fig. 13 shows the set-up, a 1-g model. The scale is 1:3 to 1:6. Peat with a water content of 300% was used for the soft soil underneath the GR in between the four piles.

A 5 cm layer of sand was applied on top of the peat and the piles. On top of this, a stiff steel frame was placed to which the GR was attached. A fill of varying height was introduced. The surcharge load was applied by a stiff load plate with a 5 cm thick water cushion underneath to distribute the surcharge load uniformly over the fill. The total load $A + B$ in the piles was measured (see Fig. 1), along with soil pressures and GR deflections. Additionally, the GR strains were measured at the locations indicated in Fig. 13 with strain gauges type 0.6/120LY1 (Hottinger Baldwin Messtechnik GmbH).

Table 9
Parameters used in the calculations for the comparison with the Oh and Shin's scaled test (2007).

Test field	Centre-to-centre distance piles $s_x = s_y$ m	Diameter pile caps d m	Height fill H m	Unit weight fill γ kN/m^3	Friction angle fill φ deg	Subgrade reaction k kN/m^3	Stiffness GR $J_x = J_y$ kN/m	Surcharge load p kPa
5	0.95	0.15	2.70	18[b]	35	236	235[a]	0
3	0.75	0.15	2.70	18[b]	35	236	235[a]	0
4	0.60	0.15	2.70	18[b]	35	236	235[a]	0

[a] Oh and Shin (2007) simulated their tests with 2D plane strain FLAC calculations using J = 800 kN/m, despite their tensile test results.
[b] This unit weight was reduced by 60% to 7.2 kN/m^3 to take into account the arching that occurs towards the test box sides as indicated in Fig. 12 and explained in section 3.10.

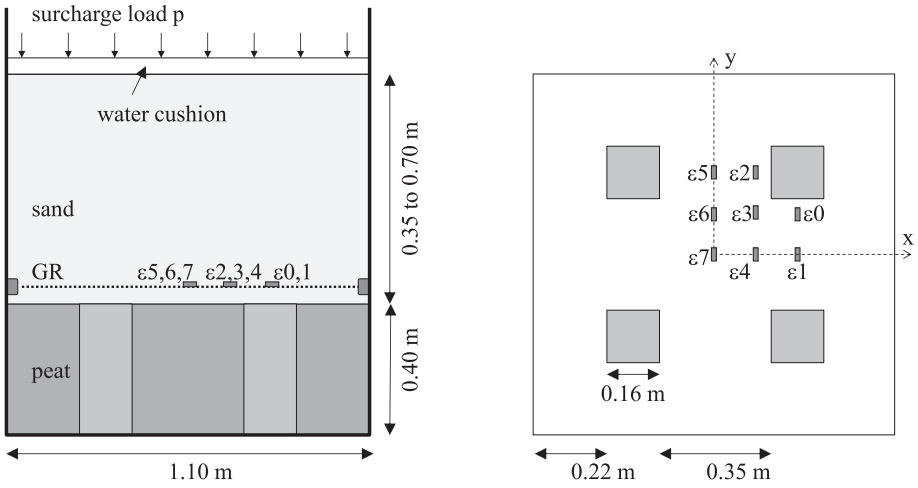

Fig. 13. Cross-section and top view of the laboratory tests reported in Zaeske (2001) and Kempfert et al. (1999, 2004), Germany. Drawing modified after Zaeske (2001).

After the installation of the fill the surcharge load was increased in steps of 8.26 kPa until the maximum top load of 124 kPa was reached. The time between each step was long enough for the primary settlement.

This paper considers four similar tests: tests 5 to 8. The fill height was 0.35 m in tests 5 and 6 and 0.70 m in tests 7 and 8. The fill consisted of poorly graded sand with $d_{50} = 0.35$ mm. The GR was 'type A' in tests 5 and 7 and 'type B' in tests 6 and 8. Type A was a knitted PET Fortrac geogrid 60/60-20; type B was PET geogrid R 30/30-12. The failure strain of PET geogrids is around 10%.

3.11.1. Determination of parameters

Short-term tensile tests according to EN 10319 showed, for GR type A, a short-term tensile stiffness $J = 1000$ kN/m for less than 1.5% strain. This was 500 kN/m for GR type B. It is not known how long each loading step was and, to stay on the 'safe side' of the prediction, the stiffness was not reduced to take the loading time into account. Reducing GR stiffness would have increased the predicted GR strain.

Fill properties were determined with triaxial testing on sand samples at 100% Proctor density (Zaeske, 2001, page 41). They are listed in Table 10.

In the calculations, the surcharge load p was reduced by 20% to take into account the friction between the box walls and the fill. Zaeske did not mention the influence of friction. Van Eekelen et al. (2012a) measured the friction in similar tests with a fill of sand. They found an average friction of 21% of the applied surcharge load. In both test series, a similar effort was made to reduce the friction with rubber sheets and grease.

The calculation value for the subgrade reaction k was determined as follows: $k = E_{peat}/t_{peat}$, where $E_{peat} = 850$ kN/m^3 (Zaeske, 2001, page 40) is the stiffness of the peat underneath the GR; and $t_{peat} = 0.40$ m is the thickness of the peat layer. This results in $k = 850/0.4 = 2125$ kN/m^3.

3.12. Laboratory scaled experiments (Van Eekelen et al., 2012a)

Van Eekelen et al. (2012a, 2013), Van Eekelen and Bezuijen (2014) reported a series of nineteen scaled laboratory experiments, which will be summarised here for the sake of clarity. Fig. 14 gives the set-up, which is a 1-g model. The scale is 1:3 to 1:5. A foam cushion modelled the soft soil around the 4 piles. This cushion was a watertight wrapped soaked foam rubber cushion. A tap was installed to drain the cushion during the test, modelling the consolidation process of the soft soil.

A 1.5–2 cm layer of sand was applied on top of the foam cushion and the piles, followed by one or two stiff steel frames to which one or two GR layers were attached. A fill of varying height was placed. The top load was applied with a water cushion that applied stresses comparable with field stresses.

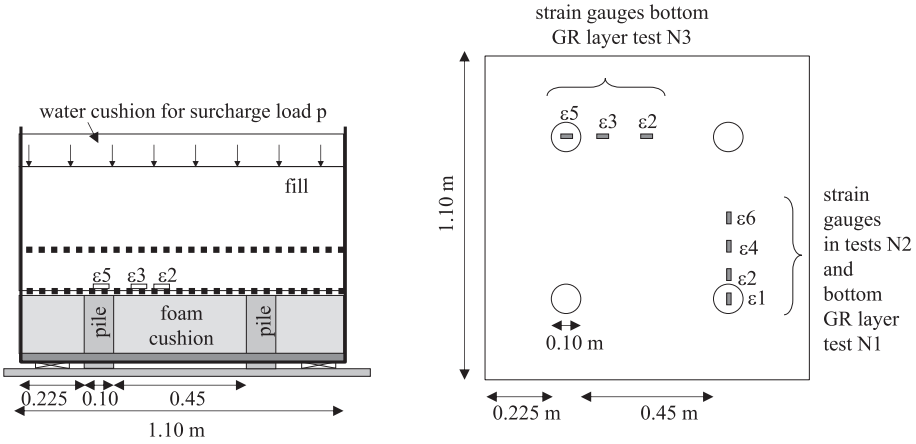

Fig. 14. Cross-section and top view of the laboratory tests reported in Van Eekelen et al. (2012a,b 2013), the Netherlands.

Table 10
Parameters used in the calculations for Zaeske's laboratory tests (2001, also reported in Kempfert et al., 2004).

Test	Centre-to-centre distance piles sx and sy m	Width square pile caps a m	Height fill H m	Unit weight fill γ kN/m3	Friction angle fill φ deg	Subgrade reaction k kN/m3	Stiffness GR along Jx kN/m	Stiffness GR across Jy kN/m	Surcharge load[a] p kPa
5	0.50	0.16	0.35	18.1	38	2125	1000	1000	0–99
6	0.50	0.16	0.35	18.1	38	2125	500	500	0–91
7	0.50	0.16	0.70	18.1	38	2125	1000	1000	0–102
8	0.50	0.16	0.70	18.1	38	2125	500	500	0–90

[a] 80% of the applied surcharge load to take into account the friction between the box walls and fill.

The test set-up was similar to Zaeske's test set-up (2001). In the series reported here, however, the fill consisted in most cases of granular material instead of sand, the subsoil support was not peat – it was controlled with the foam cushion instead – and the load distribution was measured differently so that load parts *A*, *B* and *C* could be measured separately.

Each test was carried out as follows: (1) 6 L of water was drained from the foam cushion (modelling subsoil consolidation), (2) installation of the water cushion on top of the fill followed by a first top load increase, (3) one or more drainage steps of 6 L until the subsoil support approached 0 kN/m^2, (4) second top load increase, (5) one or more drainage steps followed by top load increases of 25 kPa each until the maximum top load (usually 100 kPa) was reached and the subsequent drainage steps and (6) draining the foam cushion under vacuum to create a situation without subsoil support. There was a wait of at least two hours between each loading or drainage step to let the model stabilise.

Different GR types were installed. Only one of them, laid Secugrid PET 30/30 geogrid, was suitable for the gluing on of strain gauges. This paper presents the results of these three tests, N1, N2 and N3, which are listed in Table 11. The fill was a well-graded granular fill (crushed recycled construction material 1–16 mm). Den Boogert (2012) carried out displacement-controlled (2 mm/min) triaxial tests on three 300 mm × 600 mm samples (diameter × height) and found a peak friction angle φ_{peak} of 49.0° and a dilatation angle ψ of 9°.

3.12.1. Determination of parameters and remarks on calculations

The test geometry and fill properties are given in Table 11.

Table 12 gives the values used in the calculations for the surcharge load *p*, subgrade reaction *k*, and the GR stiffness *J* for each point just before each loading step or drainage step. The calculation value for the surcharge load was determined as follows. First, the friction *R* along the box walls was determined: $R = (\gamma H + p)\cdot s_x \cdot s_y - (A + B + C)_{measured}$. Then the calculation value for the surcharge load $p_{calculation}$ was determined as $p_{calculation} = p_{supplied} - R$.

The calculation value for the subgrade reaction *k* was determined as follows: $k = C \cdot z_{average}$, where *C* is the pressure in the subsoil-foam cushion and $z_{average}$ is the average settlement of the GR determined using the total amount of water drained from the foam cushion. In the tests, however, the subsoil support was constant. Using constant subsoil support in the calculations for, for example, test N3 instead of subgrade reaction *k* results in a difference of less than 1% in the calculated GR strain.

Each loading situation in the experiments was maintained for 2–14 h. The short-term GR stiffness, which is strain-dependent and determined with the standard quick tensile test (CEN ISO 10319) was reduced by 12% to take the loading time into account.

4. Comparison of measurements with analytical models

4.1. Analytical calculations

Table 13 gives an overview of the analytical models considered in this paper.

Strip subsoil support is considered to be unrealistic (Lodder et al. (2012), Van Eekelen et al. (2012b), Filz et al. (2012)) and is therefore considered only in a limited number of cases for the purposes of comparison.

Hewlett and Randolph's model (1988) is currently used in the French ASIRI (2012) and as a second option in the British Standard (BS8006 2010), and therefore combined with a uniformly distributed load. Neither standard allows subsoil support to be taken into account in design. However, in the present study, Hewlett and Randolph's model have been combined with subsoil support so that the results match the measurements more closely. Without subsoil support, the predicted GR strains would be larger.

In this paper, all safety factors have been disregarded. Reduction factors have been applied only to reduce strain- and time-dependent GR stiffness. This reduction was specified in each case in Section 3.

4.2. Full-scale test in Rio de Janeiro (Almeida et al., 2007, 2008)

Table 14 lists the GR strains measured by Almeida et al. (2007, 2008). These measurements confirm the assumption that the highest GR strains occur lengthwise in the GR strips. The maximum GR strain is found at the edges of the pile caps. This has also been found with measurements in the model experiments of Zaeske (2001) and Van Eekelen et al. (2012a) and numerical calculations such as those presented by Han and Gabr (2002).

The other GR strains (ε5 and ε9 on GR strips in the transverse direction; ε11 and ε12 and ε7 in the centre of four piles) were much

Table 11
Specification of the tests reported by Van Eekelen et al. (2012a and 2014) and discussed in this paper.

Test	GR	Centre-to-centre distance $s_y = s_y$ M	Diameter circular pile caps *d* m	Height fill *H* m	Height fill between 2 GR layers m	Fill unit weight γ kN/m^3	Fill friction angle φ deg
N1	2 laid PET biaxial geogrids each 30/30	0.55	0.10	0.42	0.050	15.74	49.0
N2	1 laid PET biaxial geogrid 30/30	0.55	0.10	0.42		17.24	49.0
N3	2 laid PET biaxial geogrids each 30/30	0.55	0.10	0.42	0.087	16.16	49.0

The failure strain of the applied PET biaxial geogrid is around 10%.

Table 12
Parameters used in the calculations for the laboratory experiments of Van Eekelen et al. (2012a).

Surcharge load *N1-p* kPa	Subgrade reaction *N1-k* kN/m^3	GR stiffness *N1-J* kN/m	Surcharge load *N2-p* kPa	Subgrade reaction *N2-k* kN/m^3	GR stiffness*N2-J* kN/m	Surcharge load *N3-p* kPa	Subgrade reaction *N3-k* kN/m^3	GR stiffness *N3-J* kN/m
0.00	5824	3036	0.00	649	1518	0.08	411	3036
0.00	1285	3036	6.23	1742	1518	21.57	3138	3036
8.06	736	3036	6.22	364	1518	21.13	1029	3036
21.97	1677	3036	20.62	1222	1518	20.19	421	3036
22.46	641	3036	20.05	470	1518	43.76	1332	3036
22.36	214	3036	41.20	685	1518	42.63	662	3036
43.90	881	3036				41.80	312	2634
43.52	200	3036				41.42	131	2119
42.34	246	3019				64.36	573	1754
43.93	8	2211						

Table 13
Analytical models considered.

Code for model	Arching model	Load distribution[f]	Support from subsoil underneath
Z-tri-str[g]	Zaeske[a]	Triangular[a]	GR Strip[a]
Z-inv-all		Inverse triangular[c]	all GR between piles[e]
Z-uni-all		Uniform	
HR-uni-str	Hewlett & Randolph[b]	Uniform	GR strip
CA-inv-all	Concentric Arches (CA)[d]	Inverse triangular[c]	all GR between piles
CA-uni-all		Uniform	
CA-tri-all		triangular[a]	
CA-inv-str		Inverse triangular[c]	GR Strip
CA-uni-str		Uniform	
CA-tri-str		Triangular[a]	

[a] Zaeske (2001), Kempfert et al. (2004).
[b] Hewlett and Randolph (1988).
[c] Van Eekelen et al. (2012b).
[d] Van Eekelen et al. (2013).
[e] Lodder et al. (2012).
[f] In some cases, calculations were carried out without subsoil support so that the difference between strip support and all support disappeared.
[g] *Z-tri-str* is the combination of models that is currently adopted in EBGEO (2010) and CUR (2010).

smaller, as expected. Only one exception was found: strain gauge ε7 in between four piles is surprisingly large but still smaller than the GR strains measured in and along the GR strips. A more detailed analysis of these measurements can be found in Van Eekelen et al. (2014).

The initial GR deflection or sag that occurs in this case results in relatively low GR strains (Bezuijen et al., 2010). In a comparable case without sag, more GR strain would have been measured. The cohesive fill and the initial GR sag make this case less suitable for validation. Section 5 therefore places less emphasis on the results of this case, and this was indicated with white-coloured dots in the figures in that section.

Fig. 15 compares the calculated and measured strains in and along the GR strips. As explained in section 3.2.1, a large range of values for φ have been given on the horizontal axis. Fig. 15a shows the maximum strains at the edge of the pile caps.

Both the measured and the calculated strains are larger at the edges of the pile caps than in the centre of the GR strips. As expected, all calculation models indicate that an increase in φ gives a decrease in GR strain. However, this dependency seems too strong

Table 14
Measured GR strains in Rio de Janeiro, Brazil (Almeida et al., 2007, 2008).

Edge of pile caps			On and parallel to GR strips		On GR strips, transverse direction		Centre of 4 piles, parallel to pile array		Centre of 4 piles, diagonal direction	
ε1	ε2	ε3	ε6	ε10	ε5	ε9	ε7	ε8	ε11	ε12
2.05%	1.73%	1.50%	1.50%	1.36%	0.51%	0.32%	1.14%	0.97%	0.25%	0.63%

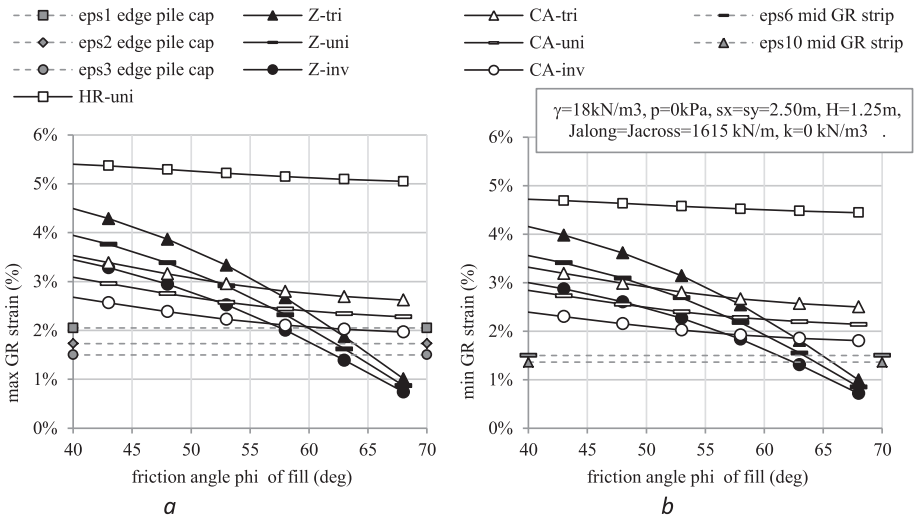

Fig. 15. Comparison of measured and calculated GR strains for the full scale test in Rio de Janeiro (Almeida et al., 2007, 2008) (*a*) GR strains at the pile cap edge and (*b*) GR strains in the centre of GR strips. Calculations with three step 1 models (Fig. 2): Zaeske (2001), Hewlett and Randolph (1988) and the CA model (Van Eekelen et al., 2013) and three step 2 load distributions (Fig. 3): triangular, uniform and inverse triangular.

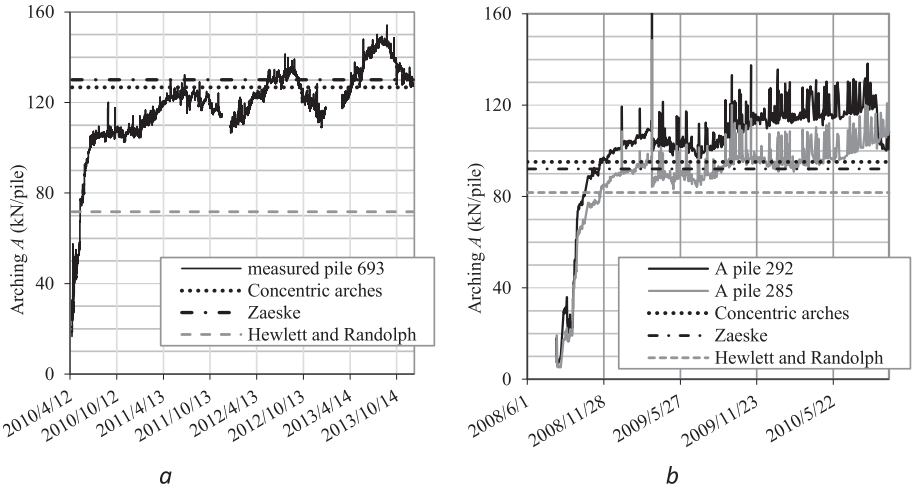

Fig. 16. Calculation step 1. Measured and calculated arching A for (a) the Woerden case (Van Eekelen et al., 2012c) and (b) the Houten case (Van Duijnen et al., 2010).

for Zaeske's arching model, resulting in very low strains for high values of φ.

Hewlett and Randolph (1988) already recommended not using their model for low embankments. Their model predicts a GR strain that is much too high. The *CA-inv* model matches the measurements best.

Generally, in design practice, it is advisable to disregard cohesion. Fig. 15 also shows the consequences of doing this, and therefore of calculating with $\varphi = 42°$. The *CA-inv* model would give a prediction that is not far from the measured value, but on the safe side. The other models give more GR strain, leading to a more conservative design.

4.3. Full-scale case in Woerden (Van Eekelen et al., 2012c)

As in the previous case, the subsoil support is negligible in this case. Fig. 16a shows the comparison of the measured and the calculated arching. The figure shows that the prediction of both the CA and the Zaeske arching model match the measurements.

The average GR strain measured between August and September 2013 was compared with the calculations in Table 15. The prediction of the inverse triangular load distributions matched the measurements well.

Fig. 17 shows measurements carried out in a tube that was installed directly upon the GR across piles 686, 687 and 688. The positions of these piles are indicated in Fig. 5. Fig. 17 also shows the second derivative of the measured shape of the GR (the tube), which is directly related to the load distribution on the GR between the piles. This second derivative shows clearly that an inverse triangular load distribution approximates the measurements better than any of the other load distributions considered.

4.4. Full-scale case in Houten (Van Duijnen et al., 2010)

Fig. 16b compares the measured and calculated arching. The predictions of both the CA and the Zaeske arching models match the measurements quite well. Further measurements have been reported by Van Duijnen et al. (2010).

Table 16 compares the measured and calculated GR strains. As explained in Section 3.4, the measured GR strains are indeed relatively high across the track and relatively low in the direction of the track. The transverse GR strains are in the same range as predicted with *CA-inv-all*. The GR strains measured along the track are so small that they have not been taken into account in the discussion in Section 5 of this paper.

The current subsoil support is greater than assumed during design. Decreasing subsoil support due to consolidation would lead to more GR strain if the load on the GR were to remain the same, both in reality and in the calculations. However, in the calculations, the load on the GR would indeed remain the same because a limit equilibrium arching model is used. In reality, the load on the GR would decrease due to increasing arching. The GR strain would therefore fall less in reality than in the calculations. For decreasing subsoil support, the relationship between measured GR strain and design model would provide additional safety: the calculated GR strains are larger than the measured values.

The inverse triangular distribution gives more strain than the uniform load distribution and, in the case of 'all subsoil', also more

Table 15
Calculated maximum GR strain and measured GR strain (average values for the period 3 August 2013–14 September 2013), 38 months after the road was opened. Case Woerden (Van Eekelen et al., 2012c).

Measured GR strain (%)							Calculated GR strain (%)[b]						
ε2			ε16		ε10		ε9			ε15		ε6	
Optic fibre	0.54	0.61	0.32	0.55	0.4	0.40							
Correction[a]	0.20	0.20	0.20	0.20	0.20	0.20	*Z-tri*	*Z-uni*	*Z-inv*	*HR-uni*	*CA-tri*	*CA-uni*	*CA-inv*
Total strain	0.74	0.81	0.52	0.75	0.67	0.60	1.18	1.01	0.86	1.97	1.25	1.08	0.92

[a] Strain before zero measurement of 4 June 2010 determined with strain cables on 9 June 2010.
[b] No subsoil support in this case, and therefore no difference between strip-subsoil and all-subsoil.

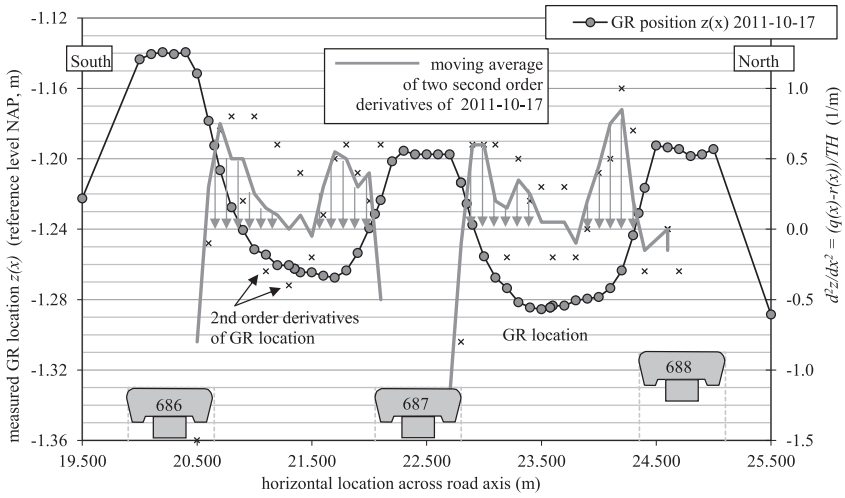

Fig. 17. Measured settlement in a tube installed upon the GR across piles 686–689, as indicated in Fig. 5, and its 2nd derivative, which is directly related to the load distribution on the GR between the piles (Case Woerden, Van Eekelen et al., 2012c).

Table 16
Average of the GR strains measured in 2010 and calculated maximum GR strains. The railway was opened in November 2008. Case Houten (Van Duijnen et al., 2010).

	Measured %	Measured %	*Z-tri-str EBGEO* %	*Z-uni-str* %	*Z-inv-str* %	*Z-tri-all* %	*Z-uni-all* %	*Z-inv-all* %	*HR-uni-str* %	*CA-tri-str* %	*CA-uni-str*%	*CA-inv-str* %	*CA-tri-all* %	*CA-uni-all* %	*CA-inv-all* %
Tranverse	$\varepsilon 1 = 0.481$	$\varepsilon 2 = 0.240$	1.08	0.88	0.82	0.32	0.31	0.49	1.12	0.99	0.80	0.75	0.28	0.28	0.44
Longitudinal	$\varepsilon 3 = 0.054$	$\varepsilon 4 = 0.024$	1.00	0.81	0.87	0.33	0.35	0.57	1.07	0.89	0.73	0.80	0.28	0.31	0.52

than the triangular load distribution. This is explained in the next section relating to the French experiments.

4.5. Large-scale French experiments (Briançon and Simon, 2012; Nunez et al., 2013)

As in the previous case, this case has a large amount of subsoil support. Arching is therefore less efficient since the differences in stiffness in the system are smaller. This results in less pressure on the piles and a more uniformly distributed pressure on the GR between the piles.

Fig. 18 compares calculated and measured GR deflection. The figure shows that taking all subsoil into account results, as expected, in a better match with the measurements. The measured GR deflection matches the *CA-uni-all* calculations best. This uniformly distributed load is combined with the counter-pressure, as shown in Fig. 19. This results in a *net* load distribution that matches the inverse triangular load distribution better than the uniform or triangular load distribution.

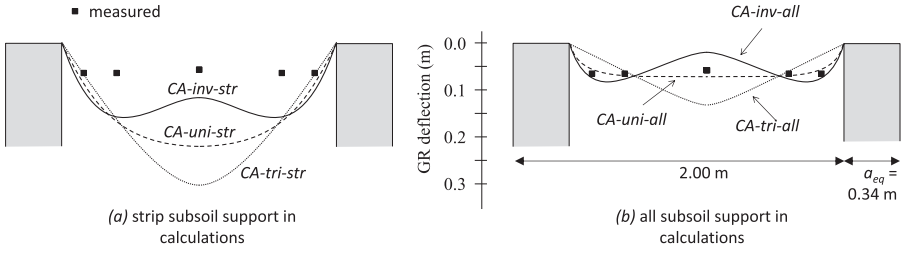

Fig. 18. Comparison of measured and calculated GR deflection in test field 3R of Briançon and Simon (2012) when $\varphi = 53°$. The measured GR deflection is the measured settlement by comparison with the settlement measured on top of the piles. Calculations with the Zaeske arching model give comparable results, as shown in Fig. 20. Measurements and calculations for test field 4R are also comparable.

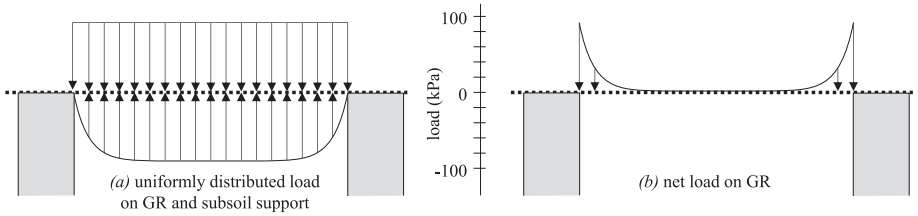

Fig. 19. Result of analytical calculation *CA-uni-all* for Briançon and Simon (2012): (a) uniformly distributed load in combination with subsoil support gives (b) a net load distribution that matches the inverse triangular load distribution in Fig. 3 better than the uniform or triangular load distribution.

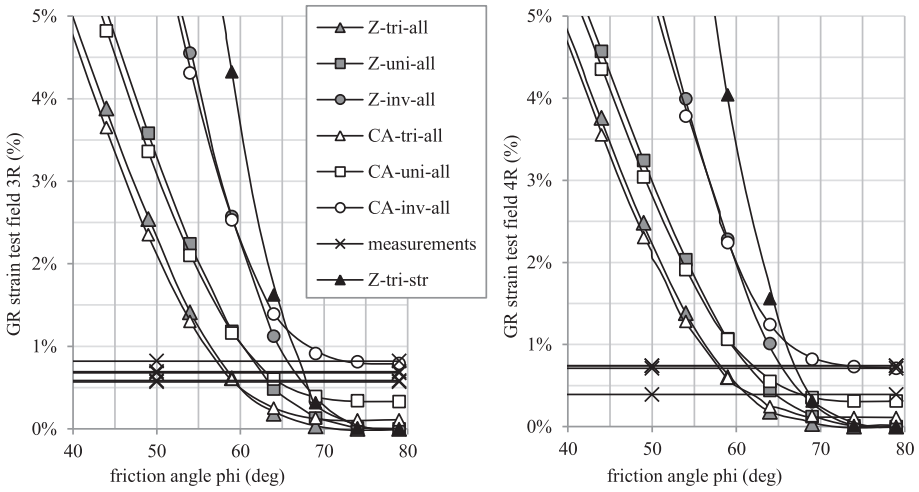

Fig. 20. Comparison of measured and calculated maximum GR strains in Briançon and Simon's full-scale field test (2012).

The calculations with inverse triangular load distribution show most GR deflection close to the piles. The resulting shape of the deformed GR leads to a relatively high GR strain. This is caused by the large counter-pressure in the centre of the GR strip, while the downwardly directed load midway between the piles is zero. This mechanism may occur in practice to a small extent, as shown by the measurements in Fig. 18. However, a stiff subsoil leads to a more uniform load distribution on top of the GR and a net load distribution that is approximately inverse triangular.

Fig. 20 compares the measured and calculated GR strains for a wide range of friction angles φ. *CA-inv-all* generally gives higher GR strains than measured, which is also the case for the other models for low friction angles.

4.6. Full-scale test and 2D DEM calculations of Huang et al. (2009)

Fig. 21a compares the measured settlement at the base of the embankment with the 2D plane strain DEM calculations of Huang et al. (2009). There is a good match. The second derivative of these derived settlements is directly related to the load distribution on the GR. Between the second and third column the second derivative matches an inverse triangular load distribution better than any of the other considered load distributions. The second derivative between the first two columns is lower and flatter. This part of the settlement tube is located below the slope of the embankment.

Fig. 21b compares the measured GR strains with the 2D plane strain DEM calculations and 3D analytical calculations. It was found that the 2D plane strain calculations with *CA-inv-all* gave nearly the same GR strain as its 3D equivalent and is therefore not shown in the figure. Note that the wall width in the 2D calculations is smaller than the column diameter in the 3D calculations, as indicated in Table 5. The 2D strains would have been smaller than the 3D strains for the same column/wall size. The figure shows a good match between measurements and several analytical calculations.

4.7. The Krimpenerwaard N210 piled embankment (Haring et al., 2008)

Table 17 shows that the measured GR strains exceed the calculated values. If the calculations are repeated with no subsoil ($k = 0$ kN/m^3), the agreement between measurements and calculations improves. The GR installation was difficult for reasons explained in Section 3.7. Otherwise, no explanation for the

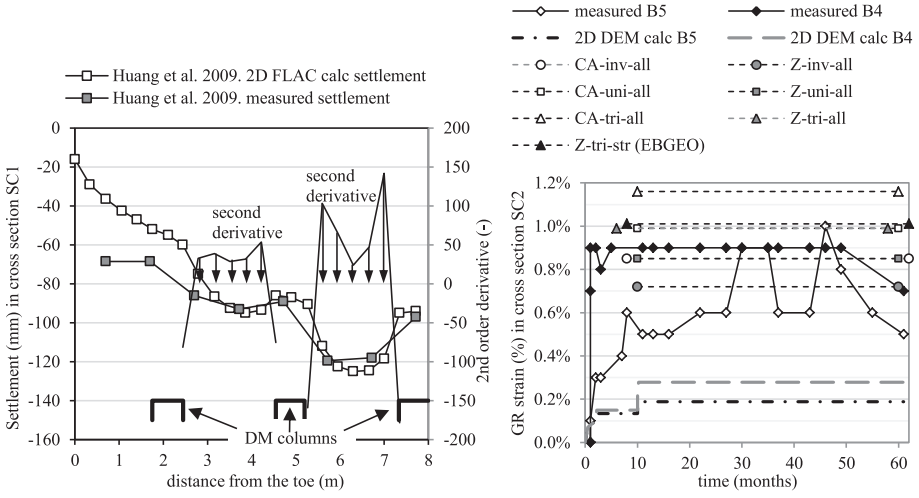

a *b*

Fig. 21. Finland. Measured and calculated (a) settlement at the base of the embankment in cross-section SC1 and (b) maximum GR strains. The left-hand picture also gives the second-order derivative of the DEM-calculated settlement; this is linearly related to the load distribution on the GR. Measurements and DEM calculations from Huang et al. (2009).

Table 17
Average of the GR strains measured in 2010 and calculated GR strains in the N210 Krimpenerwaard road, the Netherlands (Haring et al., 2008; Van Duijnen, 2014).

Average of measurements		%		Calculations							
				Subgrade	*Z-tri-str (EBGEO)*	*Z-tri-all*	*Z-uni-all*	*Z-inv-all*	*CA-tri-all*	*CA-uni-all*	*CA-inv-all*
				kN/m³	%	%	%	%	%	%	%
Longitudinal[a]	Pile cap	1.10	Longitudinal[a]	0	1.43	1.43	1.23	1.06	1.30	1.13	0.96
	Between piles	0.60		250	0.72	0.35	0.31	0.43	0.28	0.26	0.38
Transverse taking into account both GR layers	Pile cap	1.00	Transverse taking into account both GR layers	0	1.32	1.32	1.14	0.98	1.21	1.04	0.89
	Between piles	2.40		250	0.71	0.34	0.30	0.41	0.28	0.25	0.36
Transverse taking into account 1 GR layer[a]	Pile cap	1.00	Transverse taking into account 1 GR layer[a]	0	2.03	2.03	1.76	1.51	1.85	1.60	1.38
	Between piles	2.40		250	0.92	0.39	0.37	0.57	0.31	0.31	0.50

[a] These cases are included in Fig. 27.

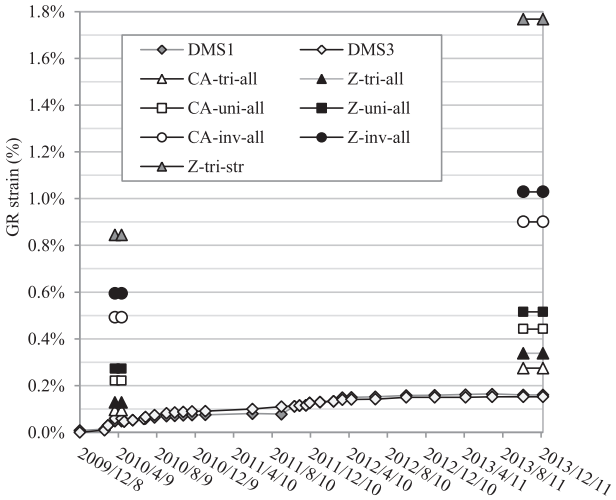

Fig. 22. Comparison of measured and calculated maximum GR strains in the full-scale field test in Hamburg (Weihbrauch, 2010, 2013). Test CSE#3 (H = 1.86 m) b. Test CSE#4 (H = 2.29 m).

discrepancy between measurements and calculations could be found.

4.8. Hamburg (Weihrauch et al., 2010, 2013)

Fig. 22 compares the measured and calculated GR strains. The figure shows that the stiff subsoil results in larger GR strains for the inverse triangular load distribution than the uniformly or triangular load distribution. An explanation is given in section 4.5.

4.9. Large-scale experiments (Sloan, 2011)

Sloan (2011) described five tests. The present paper considers the third and the fourth. In the second test, the same wire extensometers (ε) were applied as in the later tests to measure GR strains. In the second test, however, strains of up to 22% were measured. This must have been a wrong measurement because the GR would have ruptured at that GR strain. Sloan made some changes in the measurement system and believed that the strain measurements were reliable in the rest of the tests.

The tests used PP reinforcement. PP creeps. When PP reinforcement is loaded and not supported, as in these tests, it is expected that the reinforcement will creep. Fig. 23 confirms this. Seven days after dissolving the EPS, just before the loading with the small truck, the reinforcement was still creeping by 0.15–0.35% per day. After loading on day 7, creep actually accelerated. The reinforcement did not stop creeping before the end of the test. The tests are therefore not very suitable for comparison with analytical calculations and will therefore not be included in the discussion in Section 5.

However, Fig. 23 compares the measured GR strains with analytical calculations. The measured GR strains match *CA-tri* or *Z-uni* best in test CSE#3 and *CA-inv* in test CSE#4.

4.10. Oh and Shin's scaled tests (2007)

Within 2 days after the installation of the last layer of the embankment, settlement attained the maximum values and

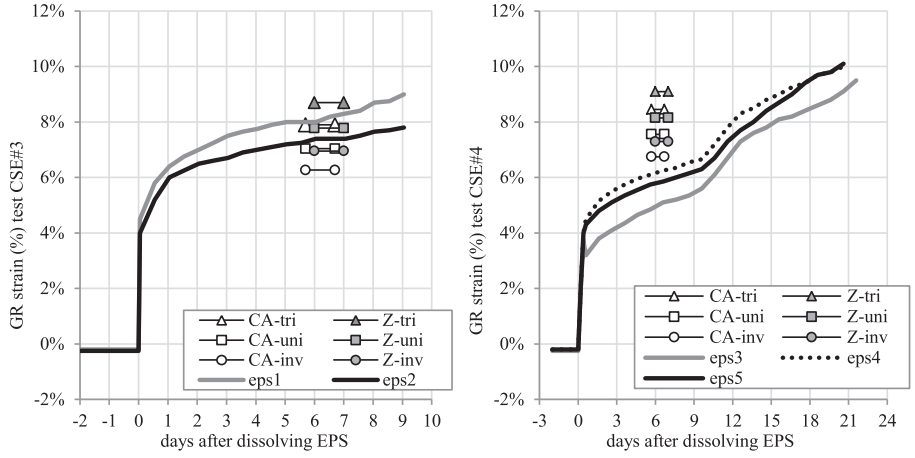

Test CSE#3 (H=1.86 m) b. Test CSE#4 (H=2.29 m)

Fig. 23. GR strains (%), comparison between measurements of Sloan (2011) and calculations.

Table 18
Measured and calculated GR strains in Korea (Oh and Shin, 2007).

ctc distance s_x (m)	GR strain	Measured	*Z-tri-str* %	*Z-tri-all* %	*Z-uni-all* %	*Z-inv-all* %	*HR-uni-str* %	*CA-tri-all* %	*CA-uni-all* %	*CA-inv-all* %
0.95	max	3.36%	10.05%	2.70%	2.95%	4.80%	10.19%	2.70%	2.95%	4.80%
0.75	max	2.44%	6.87%	2.88%	2.62%	3.50%	6.71%	2.93%	2.66%	3.54%
0.60	max	0.96%	4.61%	2.62%	2.21%	2.48%	4.29%	2.71%	2.28%	2.55%
0.95	min	1.50%	8.62%	2.61%	2.37%	3.47%	7.80%	2.61%	2.37%	3.47%
0.75	min	1.50%	6.15%	2.76%	2.24%	2.75%	5.56%	2.80%	2.28%	2.78%
0.60	min	0.68%	4.27%	2.52%	1.98%	2.09%	3.78%	2.59%	2.05%	2.14%

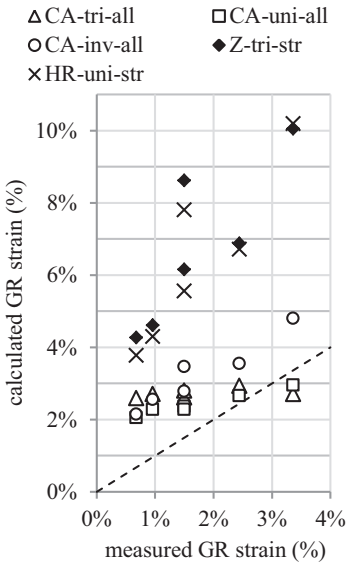

Fig. 24. Comparison of measured and calculated GR strains (%) for Oh and Shin's scaled model experiments (2007).

remained constant. Table 18 and Fig. 24 compare the measured and calculated GR strains. The 'maximum' strains were measured on top of the small pile caps. The 'minimum' strains were measured between adjacent piles. These results show that the predictions with 'all subsoil' are nearly the same for the CA and the Zaeske models. Consequently, the Zaeske predictions with 'all subsoil' are not shown in Fig. 24. The *inv* models follow the tendency of the measurements best. The strip subsoil models predict GR strains that are too high.

4.11. Laboratory scaled experiments (Zaeske, 2001; Kempfert et al., 1999, 2004)

Zaeske (2001) and Kempfert et al. (1999, 2004) showed that the largest GR strains were found in and along the GR strip. The maximum was found close to the pile cap, in other words with strain gauge ε0 (see Fig. 13). Fig. 25 therefore gives the measurements with ε0 for Zaeske's tests 5 and 7, as presented in his Figures 4.21 and 5.12 (2001). The results for tests 6 and 8 show a comparable match between measurements and calculations.

It should be noted that the measurements in Zaeske's Figures 4.21 and 5.12 do not match the measurements in Zaeske's Figure 6.19 and Figure 6 in Kempfert et al. (2004). The authors of the present paper are of the opinion that these last two figures contain some mistakes and that figures 4.21 and 5.12 give the correct measurements.

The figure shows that *Z-tri-str* (adopted in EBGEO and CUR) and *HR-uni-str* give greater GR strains than measured. Extension of the subsoil support to 'all subsoil' improves the prediction considerably. The CA model results in a better match than the Zaeske model. These tests have a relatively stiff subsoil. As explained in Section 4.5, the uniformly distributed load distribution results in the best match with the measurement, and the inverse triangular load distribution gives larger strains.

4.12. Laboratory scaled experiments (Van Eekelen et al., 2012a)

Van Eekelen et al. (2012a,b, 2013) considered step 1 and step 2 separately. Van Eekelen et al. (2012a) showed that decreasing subsoil support gives an increase in arching. This has not been found by any limit-state arching model. However, Van Eekelen et al. (2013) showed that the CA model matches the measured load distribution better than the Zaeske model.

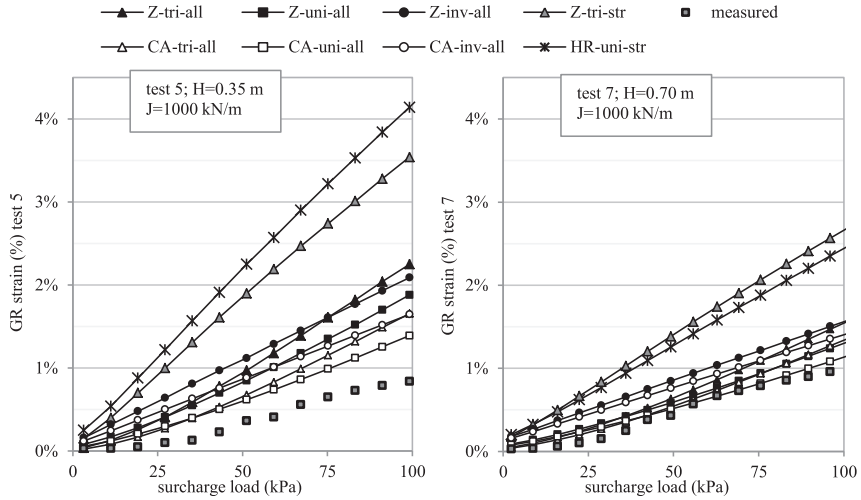

Fig. 25. GR strains (%), comparison between calculations and measurements with strain gauge ε0 (see Fig. 13) in Zaeske's laboratory experiments (2001). The surcharge load in the calculations was 80% of the applied surcharge load to compensate for the friction between the test box walls and the sand fill. This reduced load is also given on the horizontal axis.

Van Eekelen et al. (2012b) considered step 2 and showed that the measured GR strain matches the GR strain calculated with the inverse triangular load distribution and taking all the subsoil into account better.

Fig. 26 compares the measured and calculated GR strains for three experiments in which strain gauges were used. The figure shows that *CA-inv-all* matches the first two tests best. This was not the case for the third test. No explanation was found.

5. Discussion

Figs. 27 and 28 compare the measurements presented above with six combinations of calculation methods, explained in Table 13. The tests with a cohesive fill (Almeida et al., 2007; Briançon and Simon, 2012) have been included, even though they are less comparable with the analytical models developed for non-cohesive fill.

Fig. 27e and f show that *Z-tri-str* and *HR-uni-str* match the measurements least. These models overestimate the measurements with average 146% and 189%, as shown by the trendlines given in Fig. 27. Fig. 27 also shows that the Concentric Arches model (figures a and b) matches the measurements better than the Zaeske arching model (figures c and d). The average overestimation of the CA model is 16–34%, the average overestimation of the Zaeske model is 24–42%. At low friction angles, the Zaeske model generally gives higher GR strains than measured. At high friction angles, the Zaeske model gives lower GR strains than measured. This is in accordance with the findings of Van der Peet (2014) and Van der Peet and Van Eekelen (2014). They showed that the increase of

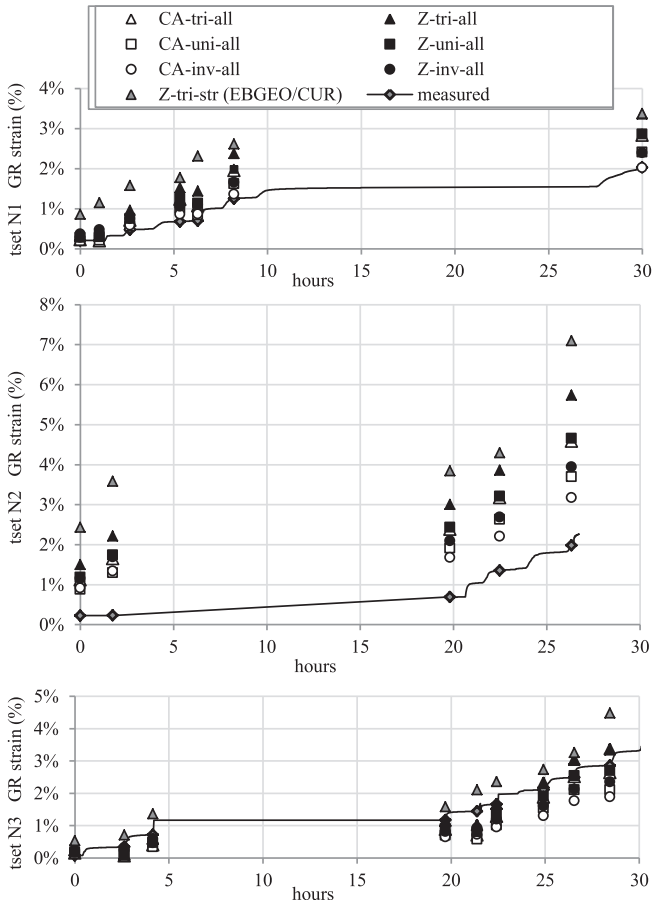

Fig. 26. GR strains (%), comparison between calculations and measurements in the laboratory experiments of Van Eekelen et al. (2012a).

arching with increasing friction angle in 3D finite-element calculations matches the CA model, while the arching in the Zaeske model increases much more strongly with increasing friction angle.

The cases with no or nearly no subsoil support are most critical as the highest GR strains will occur in relative terms. Fig. 28 therefore shows only these cases. From this figure, it can be concluded that *CA-inv-all* matches the measurements best. Thus, the inverse triangular load distribution gives the best prediction of the GR strain. This is explained as follows. If the GR deflects, the deflection is larger midway between the piles than close to the piles. The load is always attracted to stiffer elements. This is arching. A large part of the load is therefore attracted to the pile directly. However, a relatively large part is also attracted to the parts of the GR close to the piles, which deflects less and therefore seems to be stiffer.

Fig. 27 shows that the uniformly distributed load matches the measurements for the cases with subsoil support best. This is explained as follows. The differences in deflection between the different parts of the GR are smaller if the GR is partly supported by the subsoil. Less arching therefore occurs, and this is also true for the area between the piles, resulting in a more evenly distributed load.

The combination of this uniformly distributed load and counter-pressure from below results in a net load that matches the inverse triangular load distribution best, as shown in Fig. 19. In the cases where the subsoil is very stiff, the inverse triangular load distribution results in less GR deflection in the centre between piles than it is close to the pile cap edges, as can be seen in Fig. 18. This results in relatively large GR strains and therefore a relatively conservative design.

It is concluded that it is best to use an inverse triangular load distribution for the cases without, or with limited, subsoil support and a uniformly distributed load for the cases with substantial subsoil support. This can be elaborated by using the load distribution that gives the lowest value for the GR strain. In this way, a smooth transition is obtained from the situation with no subsoil support to the situation with a limited amount of subsoil support. And this gives the best match with the measurements. Fig. 29 shows that this choice results in an average overestimation of the measured values of 6%.

6. Dutch design guideline CUR 226 (2015)

The Dutch CUR committee decided to amend the Dutch CUR 226 (2010) to produce CUR 226 (2015) using the Concentric Arches model in combination with all subsoil support and the load distribution that gives the lowest GR strain. In this way, the inverse triangular distribution is applicable for the cases without, or with limited, subsoil support and a uniformly distributed load in the cases with subsoil support. A probabilistic analysis is currently being carried out, leading to a model factor with a value between 1.10 and 1.25.

Van Eekelen et al. (2013) gives the equations of the Concentric Arches model; the appendix to the current paper gives the other equations.

7. Conclusions

This paper compares several analytical models for the design of basal reinforcement in a piled embankment with case studies from literature. Three parts of the analytical models have been varied: (1) the arching model (2) the load distribution on the GR strip between adjacent piles and (3) the subsoil support. The models considered were variations on and/or extensions to the models of Hewlett and Randolph (1988) and Zaeske (2001, also reported in Kempfert et al., 2004).

Seven full-scale cases and four series of experiments have been summarised. Special attention was paid to the realistic determination of the soil parameters for the analytical calculations. Their

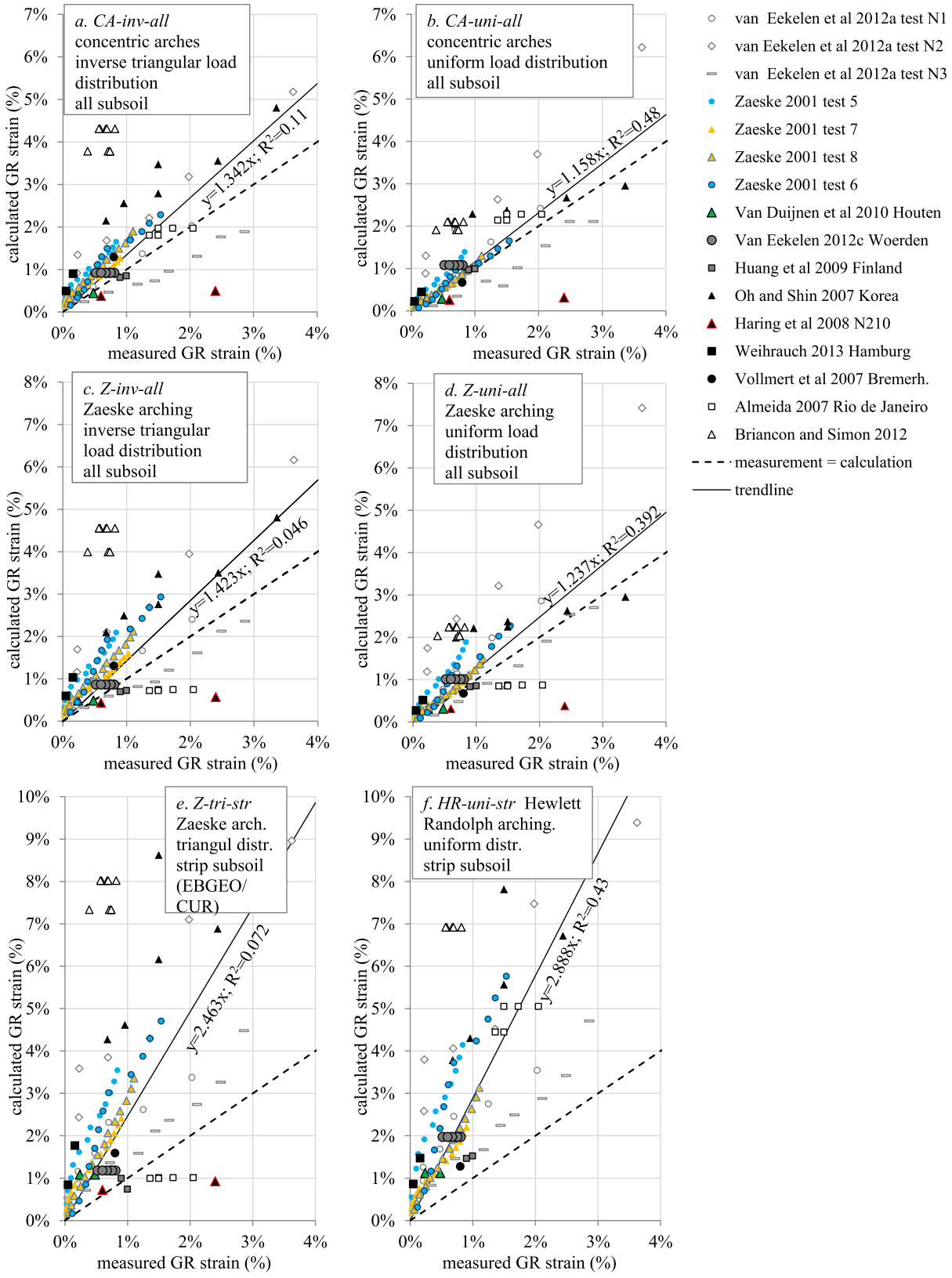

Fig. 27. Comparison of measured GR strains with results of analytical calculations, including trendline.

values should be the best guess values (mean values), not the characteristic as in design practice.

The current combination of analytical models in EBGEO and CUR226 is the arching model of Zaeske, an triangular load distribution and subsoil support below the GR strip only. BS8006 gives the option to use the combination of Hewlett and Randolph and a uniform load distribution as an alternative to the modified Marston and Anderson (1913) approach. These two combinations

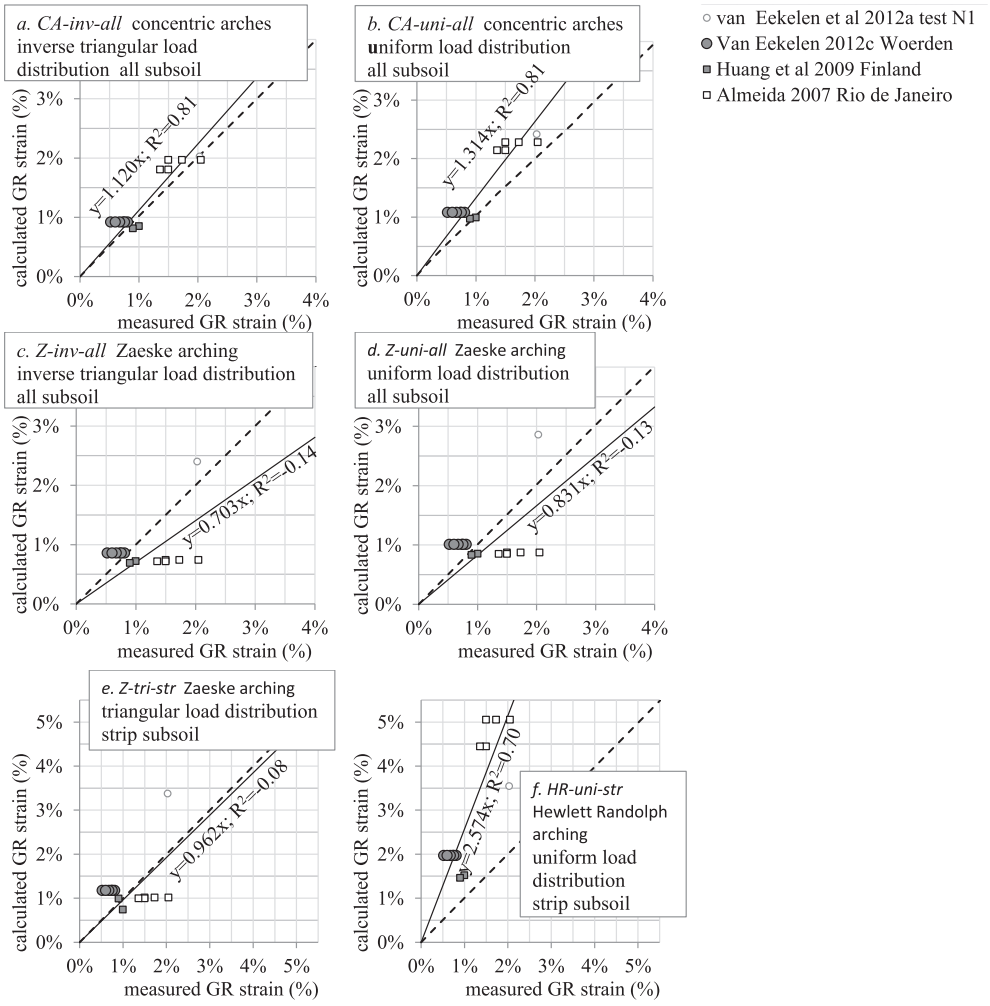

Fig. 28. Comparison of measured GR strains with results of analytical calculations; only the cases without or nearly without subsoil support have been included.

match the measurements least. They overestimate the measured strains respectively with average 146% and 189%.

The Concentric Arches model of Van Eekelen et al. (2013) gives an average overestimation of the measured GR strains of 16 to 34 %. For Zaeske's multi-scale arching model (2001) this is 24 to 42 %. From this it can be concluded that the Concentric Arches model gives GR strains that match the measurements better than Zaeske's model (2001). This conclusion holds for any load distribution. At low fill-friction angles, Zaeske's arching model generally gives low arching, leading to higher GR strains than measured. At high friction angles, Zaeske's model gives relatively high arching levels, and therefore lower GR strains than measured. Van der Peet (2014) and Van der Peet and Van Eekelen (2014) also show that Zaeske's model gives low arching for low friction angles and relatively high arching for high friction angles by comparison with their 3D numerical analyses.

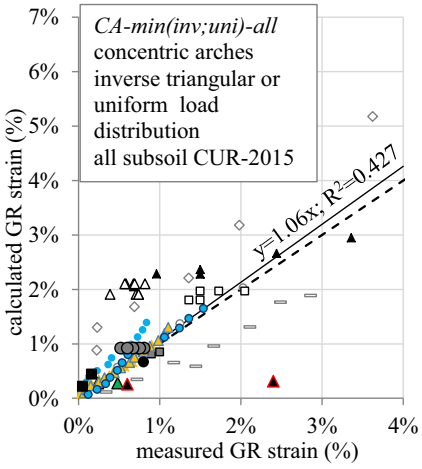

Fig. 29. Comparison of measured GR strains with results of analytical calculations; Calculation model: the minimum values *CA-inv-all* and *CA-uni-all*. This model has been adopted in CUR 226 (2015). The legend of Fig. 27 also applies to this figure.

In conditions without subsoil support, the inverse triangular load distribution gives the best prediction of the GR strain. When subsoil support is considerable, the load on the GR strip is approximately uniformly distributed. This uniform load is combined with the counter-pressure that is directed upwards. This combination results in a *net* load distribution that matches an inverse triangular load distribution more than a uniform or triangular load distribution, as shown in Fig. 19.

In the model presented by Zaeske (2001), only the subsoil underneath the GR strip between adjacent piles is taken into account. The authors have found it advisable to take all subsoil support into account. This is theoretically better, and it is also confirmed by the comparison between calculations and measurements described in the present paper.

The Dutch CUR committee decided to adapt the Dutch CUR 226 (2010) into CUR 226 (2015), using the Concentric Arches model in

combination with all subsoil support and the load distribution that gives the lowest GR strain; either the inverse triangular load distribution or the uniformly distributed load.

Acknowledgements

The financial support of Deltares and the manufacturers Naue, TenCate and Huesker for the research on piled embankments is greatly appreciated. Their financial support and fruitful debate have been extremely valuable. The authors are also grateful for additional data, analysis and discussions about the Houten case, the N210 case and several other cases with Piet van Duijnen (Huesker) and the Hamburg case (Lars Vollmert, Naue). The authors are grateful to Marijn Brugman (Arthe civil & structure) for checking all calculations given in this paper.

Appendix

Uniform load distribution

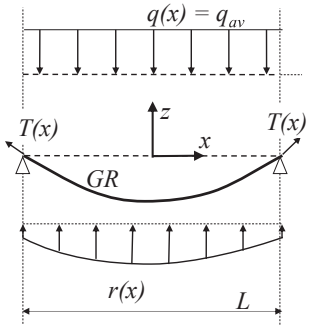

$$q_{uni}(x) = -q_{av}$$
$$z_{uni}(x) = -\frac{q_{av}}{K}\left(\frac{e^{\alpha x}+e^{-\alpha x}}{e^{\frac{1}{2}\alpha L}+e^{-\frac{1}{2}\alpha L}}-1\right) \quad (4)$$
$$z'_{uni}(x) = -\frac{q_{av}\alpha}{K}\left(\frac{e^{\alpha x}-e^{-\alpha x}}{e^{\frac{1}{2}\alpha L}+e^{-\frac{1}{2}\alpha L}}\right)$$

Inverse triangular load distribution

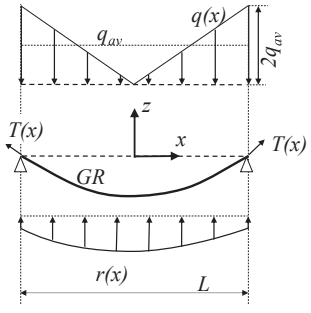

$$q_{inv}(x) = \frac{-4q_{av}}{L}\cdot x$$
$$z_{inv}(x) = -\frac{2q_{av}}{KL\alpha}\left(Me^{\alpha x}+(M-2)e^{-\alpha x}-2\alpha x\right) \quad (5)$$
$$z'_{inv}(x) = -\frac{2q_{av}}{KL}\left(Me^{\alpha x}-(M-2)e^{-\alpha x}-2\right)$$
$$\text{where } M = \frac{L\alpha+2e^{-\frac{1}{2}\alpha L}}{e^{\frac{1}{2}\alpha L}+e^{-\frac{1}{2}\alpha L}}$$

Without subsoil support ($K = 0$ kN/m^3):

$$z_{inv}(x) = -\frac{q_{av}L_w^2}{12T_H}\left(8\left(\frac{x}{L_w}\right)^3-1\right)$$
$$z'_{inv}(x) = -\frac{2q_{av}L_w}{T_H}\cdot\left(\frac{x}{L_w}\right)^2$$

Where $z(x)$ (m) is the GR deflection, L (m) is the clear distance between adjacent pile caps ($L_x = s_x - a_{eq}$) and α^2 (m^{-2}) is given by:

$$\alpha^2 = \frac{K}{T_H} \quad (6)$$

Where the subgrade reaction coefficient k (kN/m^3) is changed as follows into K (kN/m^3) to take into account all subsoil support (following Lodder et al., 2012 and Van Eekelen et al., 2012b):

$$K = \frac{A_{L_{x,y}}\cdot k}{L_{x,y}\cdot B_{ers}} \quad (7)$$

And $A_{Lx,y}$ (m^2) is the GR area belonging to a GR strip in x or y direction:

$$A_{Lx} = \frac{1}{2}\cdot(s_x\cdot s_y)-\frac{d^2}{2}\cdot\arctan\left(\frac{s_y}{s_x}\right)$$
$$A_{Ly} = \frac{1}{2}\cdot(s_x\cdot s_y)-\frac{d^2}{2}\cdot\arctan\left(\frac{s_x}{s_y}\right) \quad (8)$$

with arctan in radials, d (m) is the pile cap diameter, $q(x)$ (kPa) is the distribution load on the GR strips between adjacent piles and q_{av} (kPa) is the average load on the GR strip:

$$q_{av} = \frac{B+C}{A_{GRstrip\ transversal}+A_{GRstrip\ longitudinal}} \quad (9)$$

Where $B + C$ (kN/pile) is the total vertical load on the geosynthetic reinforcement. This value can be calculated with the equations given in Van Eekelen et al., 2013. The tensile force $T(x)$ in the geosynthetic reinforcement (kN/m) can be calculated as:

$$T(x) = T_H\sqrt{1+(z'(x))^2} \quad (10)$$

The maximum tensile force occurs at the edge of the pile cap. The value of T_H can be solved by equalising the average geometric and constitutive strain:

$$\varepsilon_{geometric,average} = \frac{\int_{x=0}^{x=\frac{1}{2}L} dx\sqrt{1+\left(\frac{dz}{dx}\right)^2}-\frac{1}{2}L}{\frac{1}{2}L}$$
$$= \varepsilon_{constitutive,average} = \frac{\frac{1}{J}\int_{x=0}^{x=\frac{1}{2}L} T(x)dx}{\frac{1}{2}L} \quad (11)$$

References

Almeida, M.S.S., Ehrlich, M., Spotti, A.P., Marques, M.E.S., 2007. Embankment supported on piles with biaxial geogrids. Geotech. Eng. 160 (4), 185–192.

Almeida, M.S.S., Marques, M.E.S., Almeida, M.C.F., Mendonca, M.B., 2008. Performance on two low piled embankments with geogrids at Rio de Janeiro. In: Proceedings of the First Pan American Geosynthetics Conference and Exhibition, Cancun, Mexico, pp. 1285–1295.

ASIRI, 2012. Recommandations pour la conception, le dimensionnement, l'exécution et le contrôle de l'amélioration des sols de fondation par inclusions rigides, ISBN 978-2-85978-462-1.

Bezuijen, A., Van Eekelen, S.J.M., Van Duijnen, P.G., 2010. Piled embankments, influence of installation and type of loading. In: Proceedings of the 9th International Conference on Geosynthetics, Brazil, 2010, pp. 1921–1924.

Blanc, M., Rault, G., Thorel, L., Almeida, M., 2013. Centrifuge investigation of load transfer mechanisms in a granular mattress above a rigid inclusions network. Geotext. Geomemb. 36, 92–105.

Blanc, M., Thorel, L., Girout, R., Almeida, M., 2014. Geosynthetic reinforcement of a granular load transfer platform above rigid inclusions; comparison between centrifuge testing and analytical modelling. Geosynth. Int. 21 (1), 37–52.

BS8006–1, 2010. Code of Practice for Strengthened/reinforced Soils and Other Fills. British Standards Institution, ISBN 978-0-580-53842-1.

Briançon, L., Simon, B., 2012. Performance of pile-supported embankment over soft soil: full-scale experiment. J. Geotech. Geoenviron. Eng 138, 551–561.

Britton, E.J., Naughton, P.J., 2008. An experimental investigation of arching in piled embankments. In: Proceedings of the 4th European Geosynthetics Congress EuroGeo 4. Edinburgh. Paper number 106.

Britton, E.J., Naughton, P.J., 2010. An experimental study to determine the location of the critical height in piled embankments. In: Proceedings of the 9th Conference on Geosynthetics, Brazil, 1961-1964.

Carlsson, B., 1987. Reinforced Soil, Principles for Calculation, Terratema AB, Linköping (in Swedish).

CEN EN ISO 10319, 2008. Geosynthetics – Wide-width Tensile Test. NEN, Delft, Netherlands.

Chen, Y.M., Cao, W.P., Chen, R.P., 2008. An experimental investigation of soil arching within basal reinforced and unreinforced piled embankments. Geotext. Geomemb. 26, 164–174.

Collin, J.G., 2004. Column supported embankment design considerations. In: 52nd Annual Geotechnical Engineering Conference – University of Minnesota.

CUR 226, 2010. Ontwerprichtlijn paalmatrassystemen (Design Guideline Piled Embankments), ISBN 978-90-376-0518-1 (in Dutch).

CUR 226, 2015. Ontwerprichtlijn paalmatrassystemen (Design Guideline Piled Embankments) updated version, to be published in 2015 (in Dutch).

Deb, K., 2010. A mathematical model to study the soil arching effect in stone column-supported embankment resting on soft foundation soil. Appl. Math. Model. 34, 3871–3883.

Deb, K., Mohapatra, S.R., 2013. Analysis of stone column-supported geosynthetic-reinforced embankments. Appl. Math. Model. 37 (5), 2943–2960.

Den Boogert, Th, Van Duijnen, P.G., Van Eekelen, S.J.M., 2012. Numerical analysis of geosynthetic reinforced piled embankment scale model tests. Plaxis Bull. 31, 12–17.

(in German) EBGEO, 2010. Empfehlungen für den Entwurf und die Berechnung von Erdkörpern mit Bewehrungen aus Geokunststoffen e EBGEO, vol. 2. German Geotechnical Society, Auflage, ISBN 978-3-433-02950-3. Also available in English: Recommendations for Design and Analysis of Earth Structures using Geosynthetic Reinforcements e EBGEO, 2011. ISBN 978-3-433-02983-1 and digital in English ISBN 978-3-433-60093-1.

Ellis, E., Aslam, R., June 2009a. Arching in piled embankments. Comparison of centrifuge tests and predictive methods, part 1 of 2. Ground Eng. 34–38.

Ellis, E., Aslam, R., July 2009b. Arching in piled embankments. Comparison of centrifuge tests and predictive methods, part 2 of 2. Ground Eng. 28–31.

Eskişar, T., Otani, J., Hironaka, J., 2012. Visualization of soil arching on reinforced embankment with rigid pile foundation using X-ray CT. Geotext. Geomemb. 32, 44–54.

Filz, G., Sloan, J., McGuire, M., Collin, J., Smith, M., 2012. Column-supported embankments: settlement and load transfer. Geotech. Eng. State Art Pract. 54–77. http://dx.doi.org/10.1061/9780784412138.0003.

Filz, G., Sloan, J., 2013. Load distribution on geosynthetic reinforcement in column-supported embankments, published. In: Proceedings of Geo-Congress, March 2013, California.

Forsman, J., Honkala, A., Smura, M., 1999. Hertsby case: a column stabilized and geotextile reinforced road embankment on soft subsoil. In: Bredenberg, H., Holm, G., Broms, B.B. (Eds.), Dry Mix Method for Deep Soil Stabilization. Balkema, Rotterdam, The Netherlands, pp. 263–268.

Forsman, J., 2001. Geovahvistetutkimus, koerakenteiden loppuraportti 1996–2001 Georeinforcement-projcet, Final Report of Test Structures 1996–2001, Tiehallinto, Helsinki, Finland (in Finnish).

Halvordson, K.A., Plaut, R.H., Filz, G.M., 2010. Analysis of geosynthetic reinforcement in pile-supported embankments. Part II: 3D cable-net model. Geosynth. Int. ISSN: 1072-6349 17 (2), 68–76. E-ISSN: 1751-7613.

Han, J., Gabr, M.A., January 2002. Numerical analysis of geosynthetic-reinforced and pile-supported earth platforms over soft soil. J. Geotech. Geoenviron. Eng. 44–53.

Haring, W., Profittlich, M., Hangen, H., 2008. Reconstruction of the national road N210 Bergambacht to Krimpen a.d. IJssel, NL: design approach, construction experiences and measurement results. In: Proceedings 4th European Geosynthetics Conference, September 2008, Edinburgh, UK.

Hewlett, W.J., Randolph, M.F., April 1988. Analysis of piled embankments. Ground Eng. 22 (3), 12–18.

Hong, W.P., Lee, J., Hong, S., 2014. Full-scale tests on embankments founded on piled beams. J. Geotech. Geoenviron. Eng. http://dx.doi.org/10.1061/(ASCE)GT.1943-5606.0001145 , 04014067.

Huang, J., Han, j., Oztoprak, S., 2009. Coupled mechanical and hydraulic modeling of geosynthetic-reinforced column-supported embankments. J. Geotech. Geoenviron. Eng 135, 1011–1021.

Jones, B.M., Plaut, R.H., Filz, G.M., 2010. Analysis of geosynthetic reinforcement in pile-supported embankments. Part I: 3D plate model. Geosynth. Int. ISSN: 1072-6349 17 (2), 59e67. E-ISSN: 1751-7613.

Jones, C.J.F.P., Lawson, C.R., Ayres, D.J., 1990. Geotextile reinforced piled embankments. In: Hoedt, Den (Ed.), Geotextiles, Geomembranes and Related Products. Balkema, Rotterdam, ISBN 90 6191 119 2, pp. 155–160.

Kempfert, H.G., Zaeske, D., Alexiew, D., 1999. Interactions in reinforced bearing layers over partial supported underground. In: Barends, et al. (Eds.), Geotechnical Engineering for Transportation Infrastructure. Balkema, Rotterdam, ISBN 90 5809 047 7.

Kempfert, H.G., Göbel, C., Alexiew, D., Heitz, C., 2004. German recommendations for reinforced embankments on pile-similar elements. In: Proceedings of EuroGeo 3, Munich, pp. 279–284.

Lally, D., Naughton, P.J., 2012. An investigation of the arching mechanism in a geotechnical centrifuge. In: Proceedings 5th European Geosynthetics Congress. Valencia, vol 5, pp. 363–367.

Le Hello, B., Villard, P., 2009. Embankments reinforced by piles and geosynthetics – numerical and experimental studies with the transfer of load on the soil embankment. Eng. Geol. 106, 78–91.

Lodder, H.J., van Eekelen, S.J.M., Bezuijen, A., 2012. The influence of subsoil reaction in a basal reinforced piled embankment. In: Proceedings of Eurogeo5, Valencia, vol. 5.

Marston, A., Anderson, A.O., 1913. The Theory of Loads on Pipes in Ditches and Tests of Cement and Clay Drain Tile and Sewer Pipe. In: Bulletin No. 31, Engineering Experiment Station.

McGuire, M.P., Filz, G.M., Almeida, M.S.S., 2009. Load-displacement compatibility analysis of a low-height column-supported embankment. In: Proceedings of IFCEE09, Florida, pp. 225–232.

McGuire, M., Sloan, J., Collin, J., Filz, G., 2012. Critical height of column-supported embankments from bench-scale and field-scale tests. In: ISSMGE – TC 211 International Symposium on Ground Improvement IS-GI Brussels.

McKelvey, J.A., 1994. The anatomy of soil arching. Geotext. Geomemb. 13, 317–329.

Naughton, P., 2007. The significance of critical height in the design of piled embankments. Soil Improv. 1–10. http://dx.doi.org/10.1061/40916(235)3.

Nunez, M.A., Briançon, L., Dias, D., 2013. Analyses of a pile-supported embankment over soft clay: full-scale experiment, analytical and numerical approaches. Eng. Geol. 153, 53–67.

Oh, Y.I., Shin, E.C., 2007. Reinforced and arching effect of geogrid-reinforced and pile-supported embankment on marine soft ground. Mar. Geores. Geotechnol. 25, 97–118.

Plaut, R.H., Filz, G.M., 2010. Analysis of geosynthetic reinforcement in pilesupported embankments. Part III: axisymmetric model. Geosynth. Int. ISSN: 1072-6349 17 (2), 77e85. E-ISSN: 1751-7613.

Public Work Research Center, 2000. Manual on Design and Execution of ReinforcedSoil Method with Use of Geotextiles, second ed. Public Work Research Center, pp. 248–256 (in Japanes).

Rogbeck, Y., Gustavsson, S., Södergren, I., Lindquist, D., 1998. Reinforced piled embankments in Sweden – design aspects. In: Proceedings of the Sixth International Conference on Geosynthetics, pp. 755–762.

Russell, D., Pierpoint, N., November 1997. An assessment of design methods for piled embankments. Ground Eng. 39–44.

Sloan, J.A., 2011. Column-supported Embankments: Full-scale Tests and Design Recommendations. PhD thesis. Virginia Polytechnic Institute and State University, Blacksburg, VA.

Spotti, A.P., 2006. Monitoring Results of a Piled Embankment with Geogrids (in Portuguese). ScD Thesis. COPPE/UFRJ, Rio de Janeiro, Brazil.

Svanø, G., Ilstad, T., Eiksund, G., Want, A., 2000. Alternative calculation principle for design of piled embankments with base reinforcement. In: Proceedings of the 4.th GIGS in Helsinki.

Terzaghi, K., 1943. Theoretical Soil Mechanics. John Wiley and Sons, New York.

Van der Peet, T.C., 2014. Arching in Basal Reinforced Piled Embankments, Numerical Validation of the Concentric Arches Model. MSc thesis. Delft University of Technology, Delft, the Netherlands.

Van der Peet, T.C., Van Eekelen, S.J.M., 2014. 3D numerical analysis of basal reinforced piled embankments. In: Proceedings of the 10th International Conference on Geosynthetics (10 ICG) in Berlin. Paper number 112.

Van der Stoel, A.E.C., Brok, C., De Lange, A.P., Van Duijnen, P.G., 2010. Construction of the first railroad widening in the Netherlands on a load transfer platform (LTP). In: Proceedings of 9 ICG, Brazil, pp. 1969–1972.

Van Duijnen, P.G., Van Eekelen, S.J.M., Van der Stoel, A.E.C., 2010. Monitoring of a railway piled embankment. In: Proceedings of 9 ICG, Brazil, pp. 1461–1464.

Van Duijnen, P.G., 2014. Personal Communication.

Van Eekelen, S.J.M., Bezuijen, A., Oung, O., 2003. Arching in piled embankments; experiments and design calculations. In: Proceedings of Foundations: Innovations, Observations, Design and Practice, pp. 885–894.

Van Eekelen, S.J.M., Bezuijen, A., Alexiew, D., 2010a. The Kyoto road piled embankment: $3^1/_2$ years of measurements. In: Proceedings of 9 ICG, Brazil, pp. 1941–1944.

Van Eekelen, S.J.M., Jansen, H.L., Van Duijnen, P.G., De Kant, M., Van Dalen, J.H., Brugman, M.H.A., Van der Stoel, A.E.C., Peters, M.G.J.M., 2010b. The Dutch design guideline for piled embankments. In: Proceedings of 9 ICG, Brazil, pp. 1911–1916.

Van Eekelen, S.J.M., Bezuijen, A., Van Tol, A.F., 2011. Analysis and modification of the British Standard BS8006 for the design of piled embankments. Geotext. Geomemb. 29, 345–359.

Van Eekelen, S.J.M., Bezuijen, A., Lodder, H.J., van Tol, A.F., 2012a. Model experiments on piled embankments Part I. Geotext. Geomemb. 32, 69–81.
Van Eekelen, S.J.M., Bezuijen, A., Lodder, H.J., van Tol, A.F., 2012b. Model experiments on piled embankments. Part II. Geotext. Geomemb. 32, 82–94 including its corrigendum: Van Eekelen, S.J.M., Bezuijen, A., Lodder, H.J., van Tol, A.F., 2012b2. Corrigendum to 'Model experiments on piled embankments. Part II' [Geotextiles and Geomembranes volume 32 (2012) pp. 82–94]. Geotextiles and Geomembranes 35: 119.
Van Eekelen, S.J.M., Bezuijen, A., van Duijnen, P.G., 2012c. Does a piled embankment 'feel' the passage of a heavy truck? High frequency field measurements. In: Proceedings of the 5th European Geosynthetics Congress EuroGeo 5. Valencia, Digital version vol. 5, pp. 162–166.
Van Eekelen, S.J.M., Bezuijen, A., van Tol, A.F., 2013. An analytical model for arching in piled embankments. Geotext. Geomemb. 39, 78–102.
Van Eekelen, S.J.M., Bezuijen, A., 2013. Dutch research on piled embankments. to be published in. In: The Proceedings of Geo-Congress, California, March 2013.
Van Eekelen, S.J.M., Almeida, M.S.S., Bezuijen, A., 2014. European analytical calculations compared with a full-scale Brazilian piled embankment. In: Proceedings of IGS10, September 2014, Berlin, Germany. Paper number 127.
Van Eekelen, S.J.M., Bezuijen, A., 2014. Is 1 + 1 = 2? Results of 3D model experiments on piled embankments. In: Proceedings of IGS10, September 2014, Berlin, Germany. Paper number 128.
Van Eekelen, S.J.M., Bezuijen, A., Van Tol, A.F., September 2015. Axial forces in piles in piled embankments, field measurements. In: proceedings of XVI ECSMGE. Edinburgh.
Van Niekerk, A.A., Molenaar, A.A.A., Houben, L.J.M., 2002. Effect of material quality and compaction on the mechanical behaviour of base course materials and pavement performance. In: Proceedings of the 6th International Conference on the Bearing Capacity of Roads and Airfields, Lisbon, Portugal, June 2002. Swets and Zeitlinger BV, pp. 1071–1179.
Vollmert, L., Kahl, M., Giegerich, G., Meyer, N., 2007. In-situ verification of an extended calculation method for geogrid reinforced load distribution platforms on piled foundations. In: Proceedings of ECSGE 2007, Madrid, vol. 3, pp. 1573–1578.
Vollmert, L., 2014. Personal Communication.
Weihrauch, S., Oehrlein, S., Vollmert, L., 2010. Baugrundverbesserungsmassnahmen in der HafenCity Hamburg am Beispiel des Stellvertreterprojektes Hongkongstrasse. Bautechnik 87 (10), 655–659 (in German).
Weihrauch, S., Oehrlein, S., Vollmert, L., 2013. Subgrade improvement measures fort the main rescue roads in the urban redevelopment area HafenCity in Hamburg. In: Proceedings of the 18th ICSMGE, Paris.
Zaeske, D., February 2001. Zur Wirkungsweise von unbewehrten und bewehrten mineralischen Tragschichten über pfahlartigen Gründungselementen, vol. 10. Schriftenreihe Geotechnik, Uni Kassel, Heft (in German).
Zhang, L., Zhao, M., Hu, Y., Zhao, H., Chen, B., June 2012. Semi-analytical solutions for geosynthetic-reinforced and pile-supported embankment. Comput. Geotech. ISSN: 0266-352X 44, 167–175. http://dx.doi.org/10.1016/j.compgeo.2012.04.001.
Zhuang, Y., Wang, K.Y., Liu, H.L., April 2014. A simplified model to analyze the reinforced piled embankments. Geotext. Geomemb. 42 (2), 154–165.